Light mixed sneutrinos as thermal dark matter

G. Bélanger[1], M. Kakizaki[1], S. Kraml[2], E. K. Park[1,3] and A. Pukhov[4]

1) LAPTH, Univ. de Savoie, CNRS, B.P. 110, F-74941 Annecy-le-Vieux, France
2) LPSC, UJF Grenoble 1, CNRS/IN2P3, 53 Avenue des Martyrs, F-38026 Grenoble, France
3) Physikalisches Institut, Universität Bonn, Nussallee 12, D-53115 Bonn, Germany
4) Skobeltsyn Inst. of Nuclear Physics, Moscow State Univ., Moscow 119992, Russia

Abstract

In supersymmetric models with Dirac neutrino masses, a left-right mixed sneutrino can be a viable dark matter candidate. We examine the MSSM+$\tilde{\nu}_R$ parameter space where this is the case with particular emphasis on light sneutrinos with masses below 10 GeV. We discuss implications for direct and indirect dark matter searches, including the relevant uncertainties, as well as consequences for collider phenomenology.

1 Introduction

A simple extension of the Standard Model (SM) by right-handed neutrinos provides the framework for describing neutrino masses and the observed neutrino oscillations [1, 2] (for reviews see, e.g., [3, 4]). Current observations, however, do not allow to establish the Majorana or Dirac nature of neutrinos. While the smallness of the neutrino mass can be naturally explained by introducing Majorana mass terms and making use of the see-saw mechanism, Dirac masses for neutrinos with very small Yukawa couplings are a viable and interesting alternative. In supersymmetric models, one may naturally obtain very light Dirac neutrino masses from F-term SUSY breaking [5]. In addition to providing an explanation for neutrino masses, this class of supersymmetric models offers an interesting alternative dark matter (DM) candidate, the sneutrino. Indeed in these models one can generate a weak-scale trilinear $A_{\tilde{\nu}}$ term that is not proportional to the small neutrino Yukawa couplings. Thus large mixing between left-handed (LH) and right-handed (RH) sneutrinos can be induced even though the Yukawa couplings are extremely small. This is in sharp contrast with the usual MSSM where the trilinear A terms are proportional to the Yukawa couplings so that mixing effects can be neglected for the first two generations of sfermions.

The lightest sneutrino can thus become the lightest SUSY particle (LSP) and a viable thermal DM candidate. Because of the large sneutrino mixing, the mainly RH sneutrino is no longer sterile, its couplings to SM gauge and Higgs bosons are driven by the mixing with its LH partner. Sufficient mixing provides efficient annihilation so that one can obtain a value for the relic density of $\Omega h^2 \simeq 0.11$ as extracted from cosmological observations [6–8].

Direct detection (DD) experiments pose severe constraints on Dirac or complex scalar, i.e. not self-conjugated, DM particles because the spin-independent elastic scattering cross-section receives an important contribution from Z exchange, which typically exceeds experimental bounds. In the mixed sneutrino model, this cross-section is suppressed by the

sneutrino mixing angle. Therefore, on the one hand a viable sneutrino DM candidate requires enough mixing to provide sufficient pair-annihilation, on the other hand the mixing should not be too large in order not to exceed the DD limits. Here we will explore the parameter space of the model where these conditions are satisfied.

It is intriguing that a mixed sneutrino also opens the possibility for a supersymmetric DM candidate below 10 GeV. Light DM candidates have received a lot of attention recently [9–19] because of results of DD experiments that show hints of events compatible with light DM. This includes the modulation signal from DAMA [20] as well as recent results from CoGeNT [21] and CDMS [22]. The best fit values for the mass and the cross-section do not overlap when these results are interpreted as a spin-independent contribution, nevertheless analyses taking into account the signal's dependence on the DM velocity distribution have shown [12, 23, 24] that the observed events can be compatible with the null results obtained by other experiments such as Xenon [25, 26]. In addition, CRESST-II has very recently reported 32 events with an expected background of 8.7 ± 1.4, compatible with a DM mass of 15 GeV or below and a spin-independent cross-section of a few times 10^{-5} pb [27].

Whether or not these events are confirmed, the possibility of light DM with large elastic scattering cross-sections remains interesting and particularly challenging to probe because experiments suffer from a severe loss of sensitivity at low masses. Furthermore, the mixed sneutrino revives the possibility of light DM in the MSSM: although it is possible to find a light neutralino that has the right properties to satisfy DM constraints in the MSSM with non-universal gaugino masses, this scenario is incompatible with additional constraints on the model [28,29]. Indeed efficient annihilation requires additional light particles, for example a second doublet Higgs with mass in the 100 GeV range, which is strongly constrained by B-physics processes, in particular $B_s \to \mu^+\mu^-$ [30]. A light neutralino is still possible in singlet extensions of the MSSM where new Higgs singlets provide additional possibilities for efficient annihilation of the lightest neutralino [18, 31].

The phenomenology of the mixed-sneutrino model that we examine here was first investigated in [5]. Indirect detection signatures were discussed in [32], and LHC signatures in [33].[1] We extend on these analyses in several ways. First of all, in contrast to the above mentioned studies, we here concentrate on light DM with mass of about 10 GeV and below. Second, we explore the parameter space of the model that gives a consistent sneutrino DM candidate using up-to-date constraints on elastic scattering cross-sections, examining also the effects of uncertainties in, e.g., the DM velocity distribution. In our scans, we take into account radiative corrections to the SUSY and Higgs spectrum; in particular we include the 1-loop corrections to the sneutrino mass originating from the Higgs contribution, and those to the light Higgs mass originating from the large $A_{\tilde{\nu}}$ term. Moreover, we consider both the case of one and of three sneutrino flavours, assuming complete degeneracy in the three flavour case. For the allowed scenarios, we explore the consequences for DD as well as for indirect detection in photons, antiparticles and neutrinos. Finally, we explore the consequences for searches at the LHC and ILC.

We characterize the scenarios that satisfy the DD constraints, including those that are within the region favoured by CoGeNT (and maybe also CRESST). The allowed scenarios have specific characteristics which include, e.g., dominantly invisible Higgs decays. Besides, if the charged sleptons are heavier than the $\tilde{\chi}_2^0$ and $\tilde{\chi}_1^\pm$, as is the case over most of the valid parameter space, this implies dominantly invisible decays of neutralinos ($\tilde{\chi}_{1,2}^0 \to \nu\tilde{\nu}_1$) and

[1] Many more studies of sneutrino DM have been performed in other models, like models with extra singlets or models with Majorana neutrino masses, see e.g., [11, 34–49].

single-lepton decays of charginos ($\tilde{\chi}_1^\pm \to \ell^\pm \tilde{\nu}_1$).

The paper is organized as follows. Section 2 describes the framework of our analysis, giving details on the model, the mass spectrum, and radiative corrections. Section 3 then discusses collider constraints, sneutrino annihilation and direct detection. The relic density and DD predictions for the one light sneutrino case are analyzed in Section 4, including a discussion of astrophysical uncertainties. Results for three degenerate light sneutrinos are presented in Section 5. Signatures in indirect detection are discussed in Section 6 and collider signatures in Section 7. A summary and conclusions are given in Section 8. The Appendix contains Feynman rules for the relevant sneutrino interactions.

All numerical results have been obtained with `micrOMEGAs` [50, 51], linked to an appropriately modified version of `SuSpect` [52].

2 Framework

2.1 Mixed sneutrinos

The framework for our study is the model of [5] with only Dirac masses for sneutrinos. In this case, the usual MSSM soft-breaking terms are extended by

$$\Delta\mathcal{L}_{\rm soft} = m^2_{\tilde{N}_i}|\tilde{N}_i|^2 + A_{\tilde{\nu}_i}\tilde{L}_i\tilde{N}_i H_u + \text{h.c.}\,, \tag{1}$$

where $m^2_{\tilde{N}}$ and $A_{\tilde{\nu}}$ are weak-scale soft terms, which we assume to be flavour-diagonal. Note that the lepton-number violating bilinear term, which appears in case of Majorana neutrino masses, is absent. Neglecting the tiny Dirac masses, the 2×2 sneutrino mass matrix for one generation is given by

$$\mathcal{M}^2_{\tilde{\nu}} = \begin{pmatrix} m^2_{\tilde{L}} + \frac{1}{2}m_Z^2\cos 2\beta & \frac{1}{\sqrt{2}}A_{\tilde{\nu}}\, v\sin\beta \\ \frac{1}{\sqrt{2}}A_{\tilde{\nu}}\, v\sin\beta & m^2_{\tilde{N}} \end{pmatrix}. \tag{2}$$

Here $m^2_{\tilde{L}}$ is the SU(2) slepton soft term, $v^2 = v_1^2 + v_2^2 = (246\text{ GeV})^2$ with $v_{1,2}$ the Higgs vaccuum expectation values, and $\tan\beta = v_2/v_1$. The main feature of this model is that the $m^2_{\tilde{L}}$, $m^2_{\tilde{N}}$ and $A_{\tilde{\nu}}$ are all of the order of the weak scale, and $A_{\tilde{\nu}}$ does not suffer any suppression from Yukawa couplings. In the following, we will always assume $m_{\tilde{N}} < m_{\tilde{L}}$ so that the lighter mass eigenstate, $\tilde{\nu}_1$, is mostly a $\tilde{\nu}_R$. It is in fact quite natural to obtain this relation when embedding the model in a GUT scale model, because the renormalization group running of $m_{\tilde{L}}$ is governed by M_2, while for $m_{\tilde{N}}$ the running at 1 loop is driven exclusively by the $A_{\tilde{\nu}}$ term, since $\tilde{\nu}_R$ is a SM singlet.

A large $A_{\tilde{\nu}}$ term in the sneutrino mass matrix will induce a significant mixing between the LH and RH states,

$$\tilde{\nu}_1 = \cos\theta_{\tilde{\nu}}\,\tilde{\nu}_R - \sin\theta_{\tilde{\nu}}\,\tilde{\nu}_L\,, \tag{3}$$

$$\tilde{\nu}_2 = \sin\theta_{\tilde{\nu}}\,\tilde{\nu}_R + \cos\theta_{\tilde{\nu}}\,\tilde{\nu}_L\,, \tag{4}$$

where $m_{\tilde{\nu}_1} < m_{\tilde{\nu}_2}$ and the mixing angle

$$\theta_{\tilde{\nu}} = \frac{1}{2}\,\sin^{-1}\left(\frac{\sqrt{2}A_{\tilde{\nu}}\, v\sin\beta}{m^2_{\tilde{\nu}_2} - m^2_{\tilde{\nu}_1}}\right). \tag{5}$$

Notice that for fixed $\sin\theta_{\tilde{\nu}}$, $A_{\tilde{\nu}}$ is proportional to $m^2_{\tilde{\nu}_2} - m^2_{\tilde{\nu}_1}$. This means that $A_{\tilde{\nu}}$ is of the same order as other soft terms in the sneutrino sector.

A large value of $A_{\tilde{\nu}}$ can induce a large splitting between the two mass eigenstates even if $m^2_{\tilde{L}}$ and $m^2_{\tilde{N}}$ are of the same order, leading to scenarios where $m_{\tilde{\nu}_1} \ll m_{\tilde{\nu}_2}, m_{\tilde{l}_L}$. In this way, $\tilde{\nu}_1$ can naturally be driven much below the neutralino masses. The model can easily be generalized to three generations. When doing so we will neglect for simplicity any flavour mixing in the sneutrino sector.

The couplings of the mostly sterile $\tilde{\nu}_1$ are those of the LH sneutrino suppressed by a factor $\sin^2\theta_{\tilde{\nu}}$ due to mixing. In addition, there is a new direct coupling between the Higgs bosons and the LH and RH sneutrino components proportional to $A_{\tilde{\nu}}$. The couplings to the Z and light Higgs boson will play a crucial role both for annihilation processes and for the elastic scattering cross-section. The coupling of sneutrinos to neutrinos and neutralinos is dominated by the wino component of the neutralinos and will be important for the annihilation of sneutrinos into neutrinos. The relevant Feynman rules are given explicitly in the Appendix.

2.2 Particle spectrum

We assume a model with soft terms defined at the weak scale and unification of gaugino masses at the GUT scale. The latter leads to $M_2 \simeq 2M_1 \simeq M_3/3$ at the weak scale. For the sneutrino sector, we take the masses and mixing angle, $m_{\tilde{\nu}_1}$, $m_{\tilde{\nu}_2}$ and $\theta_{\tilde{\nu}}$, as input parameters, and compute the $m_{\widetilde{L}}$, $m_{\widetilde{N}}$ and $A_{\tilde{\nu}}$. This also fixes the corresponding LH charged slepton mass term; for the RH one we assume $m_{\widetilde{R}} = m_{\widetilde{L}}$. Note that this choice has no effect as concerns DM properties, but can have implications for collider searches as will be discussed in Section 7.

In the one-generation case, we assume that only the tau-sneutrino is light and all others are heavy, with soft masses of 1 TeV. In the three-generation case, on the other hand, complete degeneracy between the slepton generations is assumed.

For the squark sector, we assume a common soft mass $m_{\tilde{q}} = 1$ TeV and take $A_t = -1$ TeV in order to avoid the constraint on the light Higgs mass. Other trilinear couplings for charged sparticles are neglected. The higgsino mass, pseudoscalar Higgs mass and $\tan\beta$ are also input parameters, we fix them to $\mu = 800$ GeV, $M_A = 1$ TeV and $\tan\beta = 10$.

We use a modified version of `SuSpect` [52] for the spectrum calculation. The original `SuSpect` includes the 1-loop radiative corrections to neutralino, chargino and squark masses; corrections to Higgs masses are implemented at the two-loop level. We have extended it to include RH sneutrinos, and implemented 1-loop radiative corrections to sneutrino masses as well as those to the light Higgs mass induced by the $A_{\tilde{\nu}}$ term.

2.2.1 Radiative corrections to sneutrino masses

Let $\hat{\mathcal{M}}^2_{\tilde{\nu}}(Q)$ be the running mass matrix Eq. (2) at the renormalization point Q. Then, the pole mass matrix is given by

$$\mathcal{M}^2_{\tilde{\nu}} = \hat{\mathcal{M}}^2_{\tilde{\nu}}(Q) + \begin{pmatrix} \Delta M^2_{\tilde{\nu}LL}(Q) & \Delta M^2_{\tilde{\nu}LR}(Q) \\ \Delta M^2_{\tilde{\nu}RL}(Q) & \Delta M^2_{\tilde{\nu}RR}(Q) \end{pmatrix}, \tag{6}$$

where $\Delta M^2_{\tilde{\nu}LL}(Q)$, $\Delta M^2_{\tilde{\nu}LR}(Q)$, $\Delta M^2_{\tilde{\nu}RL}(Q)$ and $\Delta M^2_{\tilde{\nu}RR}(Q)$ are radiative corrections to the LL, LR, RL and RR components, respectively. For large $A_{\tilde{\nu}}$ terms, contributions to $\Delta M^2_{\tilde{\nu}}(Q)$'s

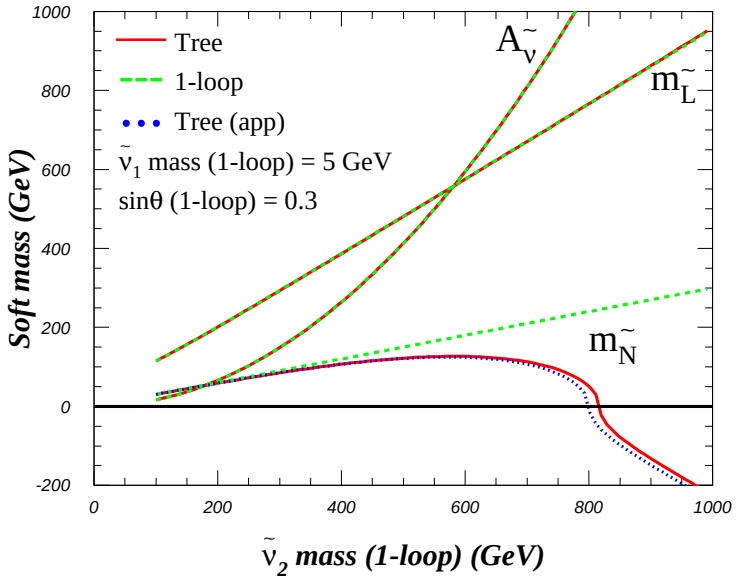

Figure 1: Tree-level and 1-loop soft terms $m_{\widetilde{L}}$, $m_{\widetilde{N}} = \text{sign}(m^2_{\widetilde{N}})|m^2_{\widetilde{N}}|^{1/2}$ and $A_{\tilde{\nu}}$ that give $m_{\tilde{\nu}_1}|_{1-\text{loop}} = 5$ GeV and $\sin\theta_{\tilde{\nu}}|_{1-\text{loop}} = 0.3$ as a function of $m_{\tilde{\nu}_2}|_{1-\text{loop}}$.

are dominated by the one–loop slepton–Higgs diagrams. The main contribution to the light sneutrino mass shift results from $\Delta M^2_{\tilde{\nu}RR}(Q)$, which can be aproximated as

$$\Delta M^2_{\tilde{\nu}RR}(Q)|_{\text{app}} = \frac{A^2_{\tilde{\nu}}}{8\pi^2}\left(\log\frac{m^2_{\tilde{\nu}_2}}{Q^2} - 1\right) . \tag{7}$$

Figure 1 shows the the sneutrino soft terms $m_{\widetilde{L}}$, $m_{\widetilde{N}}$ and $A_{\tilde{\nu}}$ that give a loop-corrected light sneutrino mass of 5 GeV and mixing angle $\sin\theta_{\tilde{\nu}} = 0.3$ as a function of $m_{\tilde{\nu}_2}$. The momentum and renormalization scales are set at $p = Q = (m_{\tilde{\nu}_1} m_{\tilde{\nu}_2})^{1/2}|_{1-\text{loop}}$. The figure also compares the complete 1-loop result (dashed green lines) to the approximation $m^2_{\tilde{\nu}_1}|_{\text{tree,app}} = m^2_{\tilde{\nu}_1}|_{1-\text{loop}} - \Delta M^2_{\tilde{\nu}RR}(Q)|_{\text{app}}$ (dotted blue lines).

2.2.2 Higgs mass corrections

After minimizing the Higgs potential, the mass of the lightest neutral Higgs reads

$$\begin{aligned} m_h^2 &= m_Z^2 \sin^2(\alpha+\beta) + m_A^2 \cos^2(\alpha-\beta) \\ &\quad + v^2\left[(\Delta\lambda_1 s_\alpha^2 c_\beta^2 + \Delta\lambda_2 c_\alpha^2 s_\beta^2 - (\Delta\lambda_3 + \Delta\lambda_4) c_\alpha s_\alpha c_\beta s_\beta \right. \\ &\qquad \left. + \Delta\lambda_5(c_\alpha^2 c_\beta^2 + s_\alpha^2 s_\beta^2) - 2(\Delta\lambda_6 s_\alpha c_\beta - \Delta\lambda_7 c_\alpha s_\beta)\cos(\alpha+\beta)\right] \end{aligned} \tag{8}$$

with $s_\alpha = \sin\alpha$, $c_\alpha = \cos\alpha$, etc.. The $\Delta\lambda_i$ include the radiative corrections to the quartic couplings. Loop diagrams involving sneutrinos can induce corrections to the quartic couplings through the presence of the weak scale $A_{\tilde{\nu}}$ term. If we neglect the Yukawa couplings of the sleptons as well as the trilinear terms for the charged sleptons, then only λ_2 receives a correction of

$$\Delta\lambda_2^{(\widetilde{\nu})} = -\frac{1}{16\pi^2}\sum_{i=1}^{N_f}\frac{|A_\nu|^4}{(m^2_{\tilde{\nu}_2} - m^2_{\tilde{\nu}_1})^2}\left(\frac{m^2_{\tilde{\nu}_2} + m^2_{\tilde{\nu}_1}}{m^2_{\tilde{\nu}_2} - m^2_{\tilde{\nu}_1}}\log\frac{m^2_{\tilde{\nu}_2}}{m^2_{\tilde{\nu}_1}} - 2\right) , \tag{9}$$

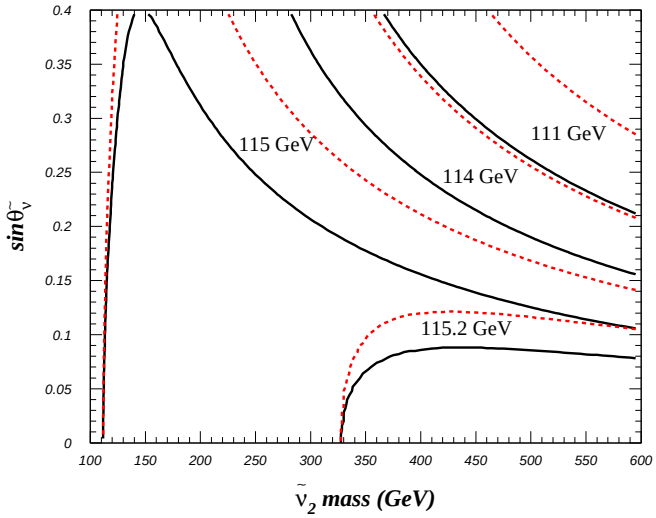

Figure 2: Contours of the radiatively-corrected light Higgs mass (from top to bottom: 111, 114, 115 and 115.2 GeV) in the $\sin\theta_{\tilde{\nu}}$ versus $m_{\tilde{\nu}_2}$ plane, for $m_{\tilde{\nu}_1} = 5$ GeV. The dotted red lines are for the case of one light sneutrino, while the full black lines are for three light sneutrino generations.

with the sum running over the sneutrino flavours, $N_f = 3$. Note that $\Delta\lambda_2^{(\tilde{\nu})}$ is negative, thus resulting in a decrease of the light Higgs mass Eq. 8. We have checked that the effective potential technique gives the same result as PBMZ [53] when $p^2 = 0$. Setting $p^2 = m_h^2$, we obtain the Higgs pole mass. We have incorporated the corrections to the light Higgs mass due to the sneutrinos in `SuSpect`. When $A_{\tilde{\nu}}$ is large (which means large mixing and a large $m_{\tilde{\nu}_2}$) the radiative corrections from the sneutrino sector can drive the light Higgs mass below the LEP limit. This is illustrated in Fig. 2, where we show contours of constant m_h in the $\sin\theta_{\tilde{\nu}}$ versus $m_{\tilde{\nu}_2}$ plane. The dotted red lines are for the case of one light sneutrino, while the full black lines are for three degenerate light sneutrinos; in either case, $m_{\tilde{\nu}_1} = 5$ GeV. Notice that the contour of $m_h = 111$ GeV for three contributing sneutrino flavours almost falls together with the $m_h = 114$ GeV contour of the one-sneutrino case.

3 Constraints on the model

3.1 Collider constraints

A light sneutrino with $m_{\tilde{\nu}} < m_Z/2$ will contribute to the invisible width of the Z boson, thus putting a constraint on the sneutrino mixing:

$$\Delta\Gamma_Z = \sum_{i=1}^{N_f} \Gamma_\nu \frac{\sin^4\theta_{\tilde{\nu}}}{2}\left(1 - \left(\frac{2m_{\tilde{\nu}}}{m_Z}\right)^2\right)^{3/2} < 2 \text{ MeV} \tag{10}$$

where $\Gamma_\nu = 166$ MeV is the partial width into one neutrino flavour. For one light sneutrino with $m_{\tilde{\nu}_1} = 5$ (20) GeV, this leads only to a mild constraint on the mixing angle of $\sin\theta_{\tilde{\nu}} < 0.39$ (0.43). In the case of three degenerate sneutrinos, this constraint becomes stricter, $\sin\theta_{\tilde{\nu}} < 0.296$ (0.33).

We also impose the limits from SUSY [54] and Higgs [55] searches at LEP2. Accounting for a theoretical uncertainty in the light Higgs mass of about 3 GeV, we require $m_h > 111$ GeV. For a large value of the sneutrino mixing this implies an upper bound on $m_{\tilde{\nu}_2}$, see Fig. 2. The radiative processes where a photon is emitted in addition to a pair of invisible supersymmetric particles will contribute to the process $e^+e^- \to \gamma + invisible$, which has been searched for by the LEP2 experiments. Here invisible particles include not only the $\tilde{\nu}_1$ but also $\tilde{\chi}_1^0$ or even $\tilde{\chi}_2^0$ when they are the NLSP and NNLSP respectively as they decay in $\tilde{\nu}_1\nu$. As the LEP2 limit we take $e^+e^- \to \gamma + invisible < 0.15$ pb at $\sqrt{s} = 189 - 209$ GeV for $p_T^\gamma > 0.02\sqrt{s}$ and $\theta_{beam\gamma} > 14$ deg [56]. We have computed the full 3-body cross-section for the single photon production using `calcHEP` [57] and found that it rarely exceeds tens of fb, which means it does not constrain our model. The reason for this is that for a large cross-section it is necessary to have a light particle exchanged in the t-channel. For neutralino production this means a light selectron, which is only possible in our 3 generation model. Likewise, $\tilde{\nu}_e\tilde{\nu}_e\gamma$ production, which is enhanced by t-channel chargino exchange, is contributing only in the 3 generation case.

In [58, 59] it was argued that the search for one-jet events with large missing transverse energy, so-called monojets, could provide a stronger limit on light DM than current DD experiments. Monojet searches at the Tevatron look for events with leading jet $p_T > 80$ GeV and missing $E_T > 80$ GeV, while 2nd jet $p_T < 30$ GeV and more jets are vetoed. An analysis [60] by the CDF collaboration of $1\,\text{fb}^{-1}$ of data gave 8449 events, with an expected background of 8663 ± 332. Using `calcHEP`, we have computed the cross-section of $p\bar{p} \to \tilde{\nu}_1\tilde{\nu}_1 + g$ at Tevatron energies and found that after cuts it is typically of the order of $0.1-1$ fb. Indeed for the parameter points that pass all other (including DD) constraints, see the scan of the following section, we find cross-sections of at most 1.5 fb. Thus the monojet search does not provide any additional constraint on the model.

In what follows, when we discuss DM allowed scenarios, it is implicitly understood that collider constraints are satisfied.

3.2 Relic abundance of sneutrino

For computing the sneutrino relic abundance, we assume the standard freeze-out picture. We do not consider non-thermal sneutrino production. This is justified because the mixed sneutrino has electroweak interactions. We have implemented the mixed sneutrino model in `micrOMEGAs 2.4`, which allows for a fully automatic computation of the annihilation and DD processes. Note that in the computation of the relic abundance we have not included the extra degrees of freedom corresponding to the RH neutrino. As these particles decouple early, this will only induce a correction at the few percent level on the effective degrees of freedom, which is negligible for our purpose.

The main annihilation channels for a light sneutrino are *i)* $\tilde{\nu}_1\tilde{\nu}_1 \to \nu\nu$ ($\tilde{\nu}_1^*\tilde{\nu}_1^* \to \bar{\nu}\bar{\nu}$) through neutralino t-channel exchange, *ii)* $\tilde{\nu}_1\tilde{\nu}_1^* \to b\bar{b}$ through exchange of a light Higgs in the s-channel, and *iii)* $\tilde{\nu}_1\tilde{\nu}_1^* \to f\bar{f}$ through Z exchange. The annihilation into neutrino pairs proceeds mainly through the wino component of the neutralino and is proportional to $\sin^4\theta_{\tilde{\nu}}$; it is largest for light winos. The Z exchange is also proportional to $\sin^4\theta_{\tilde{\nu}}$. The light Higgs exchange, on the other hand, is proportional to $(A_{\tilde{\nu}}\sin\theta_{\tilde{\nu}})^2$. Note in particular that for a fixed value of the sneutrino mixing angle, the Higgs contribution will increase with $m_{\tilde{\nu}_2}$ as $A_{\tilde{\nu}}$ also increases.

The behaviour of Ωh^2 as a function of the sneutrino mass and mixing angle is displayed

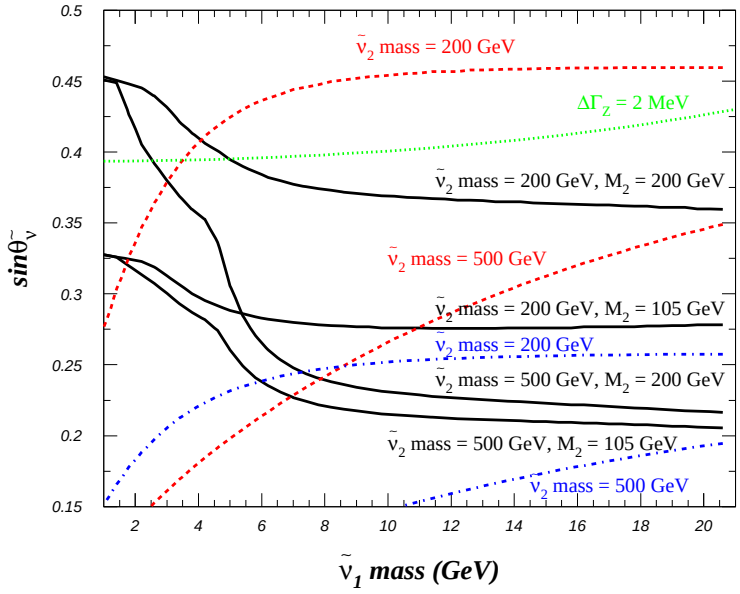

Figure 3: In black (full lines), contours of $\Omega h^2 = 0.1$ in the $\sin\theta_{\tilde{\nu}}$ versus $m_{\tilde{\nu}_1}$ plane for one light sneutrino, with $m_{\tilde{\nu}_2} = (200, 500)$ GeV and $M_2 = (105, 200)$ GeV. The remaining parameters are fixed as explained in Sec. 2.2. The dashed red and dash-dotted blue lines show contours of constant $\sigma^{\rm SI}_{\tilde{\nu}_1 N} = 10^{-4}$ pb and 10^{-5} pb, respectively. The dotted green line shows the limit from the Z width.

in Fig. 3 for the case of one light sneutrino. A larger mixing is required for light masses. This is related to the fact that Ωh^2 is inversely proportionnal to the number of degrees of freedom ($g_{\rm eff}$). At the temperature where the QCD phase transition occurs, around $T_{\rm QCD} \approx 300$MeV, the number of degrees of freedom starts to drop and Ωh^2 increases. This is relevant for DM masses below ca. 6 GeV, where the freeze-out temperature $T_f \approx m_{\rm DM}/20$ is of the order of $T_{\rm QCD}$. Furthermore note that the uncertainty in the change of $g_{\rm eff}$ around $T_{\rm QCD}$ will induce some uncertainty in the computation of Ωh^2. This is particularly important for $m_{\tilde{\nu}_1} < 2$ GeV because in this case $T_f \approx 100 - 150$ MeV, precisely where there is a sharp drop and a large uncertainty in $g_{\rm eff}$. We have not considered these corrections to the relic abundance as only a few scenarios fall in this category.

The dependence of Ωh^2 on the gaugino mass, M_2 is also displayed in Fig. 3. A lower mass requires a smaller mixing, this is because the self-annihilation channel into neutrinos is increased in this case. The relative contributions of the various annihilation channels are shown in Fig. 4 for the two cases of *a)* large mixing, $\sin\theta_{\tilde{\nu}} = 0.35$, but relatively small $A_{\tilde{\nu}}$ (left panel) and *b)* smaller mixing, $\sin\theta_{\tilde{\nu}} = 0.22$, but large $A_{\tilde{\nu}}$ (right panel). In the large $A_{\tilde{\nu}}$ case, the contribution from the Higgs exchange enhances the $b\bar{b}$ channel if kinematically accesssible.

3.3 Direct detection

The spin-independent (SI) scattering of $\tilde{\nu}_1$ on nucleons occurs through Z or Higgs exchange. The Z exchange is again suppressed by the sneutrino mixing angle. The scattering cross-

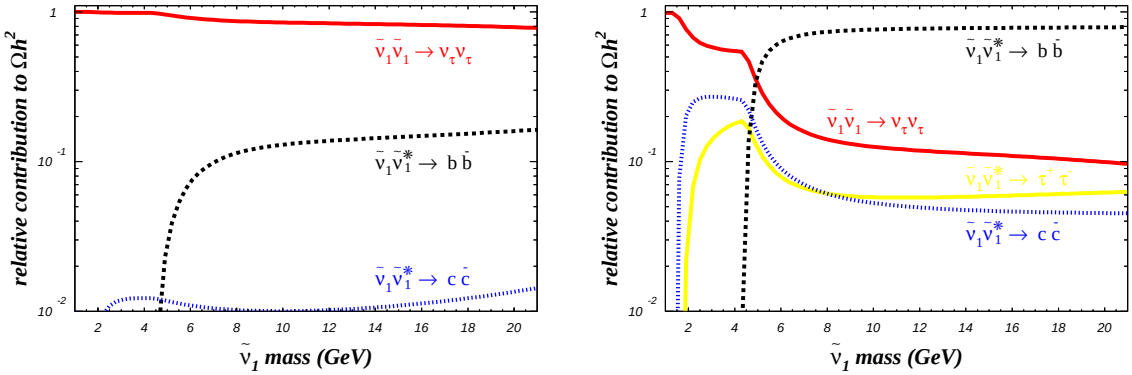

Figure 4: Relative contributions of different annihilation channels as a function of the $\tilde{\nu}_1$ mass, on the left for $m_{\tilde{\nu}_2} = 200$ GeV and $\sin\theta_{\tilde{\nu}} = 0.35$, on the right for $m_{\tilde{\nu}_2} = 500$ GeV and $\sin\theta_{\tilde{\nu}} = 0.22$, cf. Fig. 3. In both plots, $M_2 = 200$ GeV.

section on a nucleus due to Z exchange is given by

$$\sigma^{\mathrm{SI,Z}}_{\tilde{\nu}_1 N} = \frac{G_F^2}{2\pi}\mu_\chi^2\left((A-Z) - (1-4\sin^2\theta_W)Z\right)^2\sin^4\theta_{\tilde{\nu}}\,, \tag{11}$$

where μ_χ is the sneutrino–nucleus reduced mass, while A is the atomic weight and Z the number of neutrons of the nucleus. One peculiarity of the Z-exchange contribution is that the proton cross-section is much smaller than the neutron one, with the ratio of amplitudes $f_p/f_n = (1-4\sin^2\theta_W)$. The Higgs contribution on the other hand, which becomes dominant for large values of $A_{\tilde{\nu}}$, is roughly the same for protons and neutrons,

$$\sigma^{\mathrm{SI},h}_{\tilde{\nu}_1 N} = \frac{\mu_\chi^2}{4\pi}\frac{g^2_{h\tilde{\nu}_1\tilde{\nu}_1}}{m_h^4 m^2_{\tilde{\nu}_1}}\left((A-Z)\sum_q g_{hqq}f_q^n m_n + Z\sum_q g_{hqq}f_q^p m_p\right)^2\,, \tag{12}$$

where $g_{hqq} = e/(2M_W s_W)x_q$ ($x_u = -\cos\alpha/\sin\beta, x_d = \sin\alpha/\cos\beta$) is the Higgs coupling to quarks after the quark mass has been factored out, and $g_{h\tilde{\nu}_1\tilde{\nu}_1}$ is the coupling to the LSP as given in Appendix A.

The total SI cross-section is obtained after averaging over the $\tilde{\nu}_1 N$ and $\tilde{\nu}_1^* N$ cross sections, where we assume equal numbers of sneutrinos and anti-sneutrinos. Here note that the interference between the Z and Higgs exchange diagrams has opposite sign for $\tilde{\nu}_1 N$ and $\tilde{\nu}_1^* N$, leading to an asymmetry in sneutrinos and anti-sneutrinos scattering if both Z and Higgs exchange are important. We will come back to this in Section 6.1, when we discuss signals from sneutrinos captured in the Sun.

A comment is in order concerning theoretical uncertainties. The computation of the elastic scattering cross-section for the Higgs-exchange diagram depends on the quark coefficient in the nucleons, which can be determined from the pion-nucleon sigma term, $\sigma_{\pi N}$ and from the SU(3) symmetry breaking effect, $\sigma_0 = 35 \pm 5$ MeV [61]. By default we take $\sigma_0 = 35$ MeV and $\sigma_{\pi N} = 45$ MeV [61]. This leads to

$$\begin{aligned} f_d^p &= 0.026\,, \quad f_u^p = 0.020\,, \quad f_s^p = 0.13\,, \\ f_d^n &= 0.036\,, \quad f_u^n = 0.014\,, \quad f_s^n = 0.13\,. \end{aligned} \tag{13}$$

More recent estimates of the pion-nucleon sigma term typically indicate larger values of $\sigma_{\pi N} = 55 - 73$ MeV [62]. The very recent lattice results also tend towards a larger value

for the strange quark content of the nucleon, although uncertainties are still large [63, 64]. The overall theoretical uncertainty that arises from the uncertainty in the scalar coefficients is relevant only for cases where the Higgs-exchange contribution dominates, since for the Z contribution the vector coefficients are simply determined by the valence quark content in the nucleon. Since the values in Eq. (13) are rather on the low side, the DD cross-section shows a larger upward than downward variation when $\sigma_{\pi N}$ and σ_0 are varied within their allowed ranges. For example, for $(\sigma_{\pi N},\, \sigma_0) = (70,\, 30)$ MeV the cross-section can increase by up to a factor 3.5 when Higgs exchange dominates, while for (55, 35) MeV the increase is at most a factor 1.7. The choice (45, 40) MeV on the other hand implies a decrease in the cross-section that can reach 30%.

The limits on $\sigma_p^{\rm SI}$ from DD experiments are extracted from the observed limit on the LSP–nucleus scattering cross-section assuming that amplitudes for protons (f_p) and neutrons (f_n) are equal. In our model this is not the case when Z exchange dominates. Therefore, we compute instead the normalized cross-section on a point-like nucleus,

$$\sigma^{\rm SI}_{\tilde\nu_1 N} = \frac{4\mu_\chi^2}{\pi}\frac{\left(Zf_p + (A-Z)f_n\right)^2}{A^2} \tag{14}$$

where the average over $\tilde\nu_1$ and $\tilde\nu_1^*$ is assumed implicitly. This cross-section can be directly compared with the limits on $\sigma_p^{\rm SI}$ given by the experiments. For Xenon $A = 131, Z = 54$ while for Germanium $A = 76, Z = 32$.

The SI scattering cross-section mainly depends on the three parameters of the sneutrino sector as long as m_A is large enough so that heavy Higgs exchange can be neglected. Contours of constant $\sigma^{\rm SI}_{\tilde\nu_1 N}$ in the $\sin\theta_{\tilde\nu}$ versus $m_{\tilde\nu_1}$ plane are displayed in Fig. 3 for two different values of $m_{\tilde\nu_2}$. For $m_{\tilde\nu_2} = 200$ GeV, in the region $m_{\tilde\nu_1} \gtrsim 6$ GeV the $A_{\tilde\nu}$ parameter is so small that scattering proceeds mainly via the Z-boson exchange; the detection rate is almost independent of $m_{\tilde\nu_1}$. For $m_{\tilde\nu_2} = 500$ GeV, $A_{\tilde\nu}$ is so large that the nucleon scattering has an important component from the Higgs-boson exchange; for this channel the detection rate is proportional to $m_{\tilde\nu_1}^{-2}$. Therefore the detection rate gets smaller for larger $\tilde\nu_1$ mass. This is a characteristic of scalar dark matter particles. Similarly for $m_{\tilde\nu_1} < 6$ GeV, the nucleon scattering proceeds mainly through Higgs-boson exchange implying an increase for lower $\tilde\nu_1$ mass.

Before we proceed, another comment is in order concerning the $\tan\beta$ dependence. So far we have only considered $\tan\beta = 10$. The main effect of increasing $\tan\beta$ is a lower $\tilde\tau_1$ mass for the same choice of $m_{\tilde\nu_1},\ m_{\tilde\nu_2},\ \sin\theta_{\tilde\nu}$ and μ. In our approach, this can be translated into an upper limit on $\tan\beta$ as a function of $m_{\tilde\nu_2}$, or vice-versa a lower limit on $m_{\tilde\nu_2}$ as a function of $\tan\beta$. In fact, for $m_{\tilde\nu_2} = 200$ GeV like in Figs. 3 and 4, one can only go up to $\tan\beta \approx 20$; for higher values one first violates the $\tilde\tau_1$ mass bound and then gets tachyonic staus. For high values of, e.g., $\tan\beta = 50$, one needs $m_{\tilde\nu_2} \gtrsim 300$ GeV. Another effect is a slightly higher h^0 mass for higher $\tan\beta$.

The influence on the relic density of the $\tilde\nu_1$ is small, the main effect being a slight suppression of the $\tilde\nu_1\tilde\nu_1^* \to \tau^+\tau^-$ channel through the interference of the Higgs and chargino exchange diagrams. To give a concrete example, for $m_{\tilde\nu_1} = 10$ GeV, $m_{\tilde\nu_2} = 500$ GeV, $\sin\theta_{\tilde\nu} = 0.22$, $M_2 = 200$ GeV and $\tan\beta = 10$ we have $\Omega h^2 = 0.12$ with 6% contribution from $\tilde\nu_1\tilde\nu_1^* \to \tau^+\tau^-$, cf. Fig 4. For the same parameters but $\tan\beta = 50$, we get $\Omega h^2 = 0.131$ with 4% contribution from $\tilde\nu_1\tilde\nu_1^* \to \tau^+\tau^-$. Lowering M_2 to 105 GeV leads to $\Omega h^2 = 0.092$ (0.1) for $\tan\beta = 10$ (50).

The SI scattering cross-section is affected by $\tan\beta$ through the Higgs mass and the bottom Yukawa coupling, but this effect is also small. In the above example with $M_2 = 200$ GeV,

$\sigma^{\rm SI}_{\tilde{\nu}_1 p} = 8.63 \times 10^{-5}$ pb and $\sigma^{\rm SI}_{\tilde{\nu}_1 n} = 1.17 \times 10^{-4}$ pb change to $\sigma^{\rm SI}_{\tilde{\nu}_1 p} = 8.04 \times 10^{-5}$ pb and $\sigma^{\rm SI}_{\tilde{\nu}_1 n} = 1.11 \times 10^{-4}$ pb when increasing $\tan\beta$ from 10 to 50. Here note that $m_h = 114.2$ (115.2) GeV and $A_{\tilde{\nu}} = 310.7$ (309.2) GeV at $\tan\beta = 10$ (50).

We conclude that the choice of $\tan\beta$ has little influence on the results. However, lower $\tan\beta$ has more parameter space in the sense that one can go to lower $\tilde{\nu}_2$ masses. Therefore in the following we will focus on $\tan\beta = 10$.

4 Results for one light sneutrino flavour

For the light sneutrino to be a viable dark matter candidate, in addition to the collider constraints, we require that both the 3σ upper bound from WMAP5 [6], $\Omega h^2 < 0.1285$, and the DD limits be satisfied. In fact, DD here provides the more stringent constraint. We first discuss the case of one light sneutrino, concentrating on the third generation.

For the numerical analysis, we perform a random scan of the parameters of the sneutrino and gaugino sector. To search efficiently the region with a light sneutrino, we use $m_{\tilde{\nu}_{1,2}}$ and $\sin\theta_{\tilde{\nu}}$ as input, from which we compute $m_{\widetilde{L_3}}$, $m_{\widetilde{N_3}}$ and $A_{\tilde{\nu}} = A_{\tilde{\nu}_3}$. The parameter ranges we scan over are

$$\begin{aligned} &1 \text{ GeV} < m_{\tilde{\nu}_1} < 15 \text{ GeV}\,, \qquad && 100 \text{ GeV} < m_{\tilde{\nu}_2} < 1000 \text{ GeV}\,, \\ &0 < \sin\theta_{\tilde{\nu}} < 0.5\,, && 100 \text{ GeV} < M_2 = 2M_1 < 500 \text{ GeV}\,. \end{aligned} \tag{15}$$

All other parameters have little influence on the light sneutrino scenario and are therefore fixed as specified in Section 2.2. In particular, the stau masses are determined through $m_{\widetilde{R}_3} = m_{\widetilde{L}_3}$ and $A_\tau = 0$, while all other soft masses are set to 1 TeV. Moreover, having checked that it does not influence the results, we set $\mu = 800$ GeV. The scan is carried out in two steps with 50000 points each, the first varying M_2 from 100 to 150 GeV (light wino case) and the second varying M_2 from 150 to 500 GeV (heavy wino case). Extending the upper value for the range of M_2 has no influence on our results.

The scan results are shown in Fig. 5 in the $\sin\theta_{\tilde{\nu}}$ versus $m_{\tilde{\nu}_1}$ and Ωh^2 versus $m_{\tilde{\nu}_1}$ planes. We find scenarios that satisfy the WMAP and DD limits for sneutrinos as light as 1 GeV. Such light $\tilde{\nu}_1$'s below ca. 4 GeV require a large mixing, $\sin\theta_{\tilde{\nu}} \gtrsim 0.25$, and annihilate predominantly into neutrinos. A more modest mixing of $\sin\theta_{\tilde{\nu}} > 0.12$ is needed for $\tilde{\nu}_1$ masses above the b-threshold, where annihilation into $b\bar{b}$ through Z or h can contribute significantly.

Figure 6 shows the expected SI cross-sections for Xe as a function of the $\tilde{\nu}_1$ mass, together with the limits from CoGeNT, Xenon10 and Xenon100, which give the most stringent constraints on light DM [21, 25, 26]. The cross-section is appropriately re-scaled if the $\tilde{\nu}_1$ is only a part of the DM, i.e. $\xi = \Omega h^2/0.11$ for points with $\Omega h^2 < 0.0913$ and $\xi = 1$ otherwise.

When the sneutrino annihilation is dominated by Z or Higgs exchange, the prediction for the SI scattering cross-section, which is also dominated by the Z or Higgs exchange diagrams, is directly related to the annihilation cross-section. In this case, after re-scaling for the lower dark matter density if $\Omega h^2 < 0.0913$, $\sigma^{\rm SI}_{\tilde{\nu}_1 N}$ varies only within a factor of 2 (not taking into account uncertainties due to the quark coefficients Eq. (13)). On the other hand, when the sneutrino annihilates dominantly into neutrino pairs, there is no such correlation between Ωh^2 and $\sigma^{\rm SI}_{\tilde{\nu}_1 N}$, and it is possible to suppress the direct detection cross-section by more than one order of magnitude. These scenarios correspond to the scatter points with low cross-sections in Fig. 6.

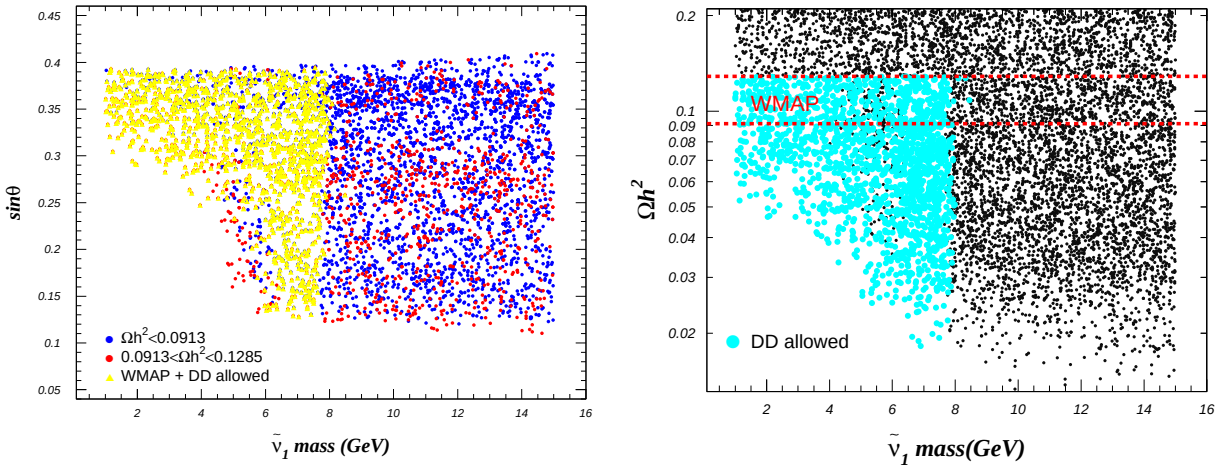

Figure 5: Scan results for the one light sneutrino case. On the left, a scatter plot of $\sin\theta_{\tilde{\nu}}$ versus $m_{\tilde{\nu}_1}$. Here the red (blue) dots show models that have a relic density within (below) the 3σ WMAP range. The yellow triangles refer to models that satisfy the WMAP upper bound as well as the DD limits from CoGeNT and Xenon10. The plot on the right shows Ωh^2 versus $m_{\tilde{\nu}_1}$ with the light blue points passing the DD constraints.

The points that successfully pass all constraints have sneutrino masses of about 1 to 8 GeV and include many scenarios that have cross-sections within the range favoured by CoGeNT. In particular the bulk of our scenarios with masses around 7–8 GeV are in the region allowed by CoGeNT and Xenon. Recall also that such light DM with a cross-section of a few times 10^{-5} pb could cause the events observed by CRESST. For $m_{\tilde{\nu}_1} \approx 5$ GeV, many of the WMAP-allowed scenarios lie above the CoGeNT limit. A value of $M_2 \sim 100 - 120$ GeV is required in this case to achieve efficient enough annihilation into neutrinos. For lower masses, the DD limit becomes much weaker, leaving the relic density and Z width as the main constraints. Moreover, we recall that, while some fine-tuning is needed to achieve a light $\tilde{\nu}_1$, there are no large hierarchies among the soft terms (cf. Section 2.1). In particular the ratio between $A_{\tilde{\nu}}$ and M_2 roughly ranges from 1/5 to 5 (8) for $m_{\tilde{\nu}_1} \lesssim 6$ (8) GeV.

It is also intriguing that in Fig. 6 there is a lower limit on the DD cross-section of about 10^{-5} pb, which is almost flat for $m_{\tilde{\nu}_1} \gtrsim 4$ GeV. It arises because the lowest $\sigma^{\rm SI}_{\tilde{\nu}_1 N}$ is obtained when the dominant contribution to the relic abundance is annihilation into neutrinos. In this case, scattering off nucleons proceeds dominantly through the Z-boson exchange, which is almost independent of $m_{\tilde{\nu}_1}$. Note that this lower limit is free of the theoretical uncertainties on the quark coefficients in the nucleon. The mild mass dependence of the lower limit on $\sigma^{\rm SI}_{\tilde{\nu}_1 N}$ for $m_{\tilde{\nu}_1} < 4$ GeV arises because the Higgs exchange which is dominant in this region, is porportional to $1/m^2_{\tilde{\nu}_1}$, Eq. (11). Overall, this lower limit means that mixed sneutrino DM with a mass of a few GeV will be either discovered or excluded if the DD experiments can cover SI cross-sections down to 10^{-5} pb.

The mass of the $\tilde{\nu}_2$ and consequently of the $\tilde{\tau}_{1,2}$ is also constrained. When M_2 is small, around ca. 100 GeV, and annihilation into neutrinos dominates, the angle $\sin\theta_{\tilde{\nu}} > 0.25$ to provide sufficient annihilation but the mass of $\tilde{\nu}_2$ is not constrained. On the other hand when Higgs exchange is dominant, the annihilation is proportionnal to $A^2_{\tilde{\nu}} \sin\theta^2_{\tilde{\nu}} \approx m^4_{\tilde{\nu}_2} \sin\theta^4_{\tilde{\nu}}$, which gives a lower bound on $m_{\tilde{\nu}_2}$. Consequently a lower bound on $m_{\tilde{\tau}_1} \gtrsim 250$ GeV is obtained for large M_2. This is illustrated in Fig. 7, which shows the points of Fig. 5 in the $m_{\tilde{\chi}^\pm_1}$ versus $m_{\tilde{\tau}_1}$

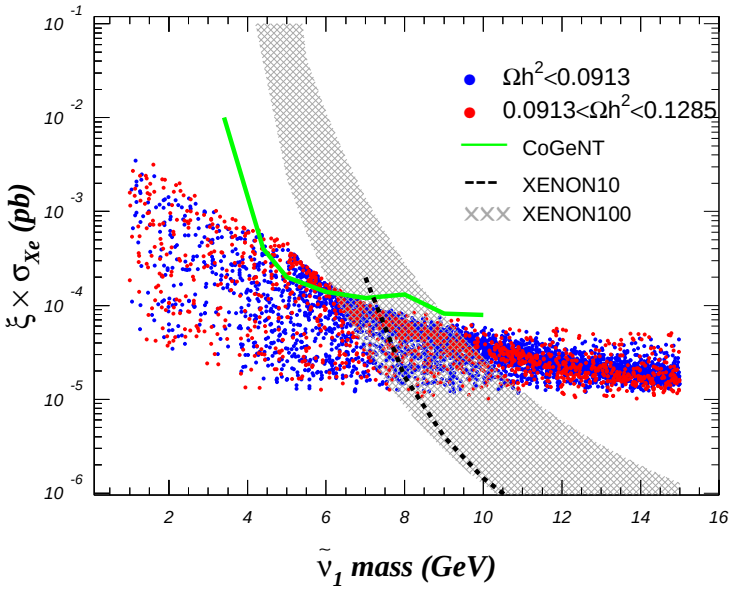

Figure 6: Scatter plot of re-scaled $\sigma^{\rm SI}_{\tilde{\nu}_1 Xe}$ as a function of $m_{\tilde{\nu}_1}$ for the case of one light sneutrino. The red (blue) dots show models that are within (below) the WMAP range. Also shown are the limits from CoGeNT (green), Xenon10 (dashed), and Xenon100 limit (crosses). The CoGeNT and Xenon10 limits are for $v_0 = 220$ km/s, $v_{esc} = 600$ km/s and $\rho = 0.3$ GeV/cm^3. The Xenon100 band is obtained by varying $v_0 = 180$–260 km/s, $v_{esc} = 500$–600 km/s, $\rho = 0.2$–0.6 GeV/cm^3 and an $L_{\rm eff}$ that decreases at low energies, see Sec. 4.1 for details.

plane. We found a few scenarios with $m_{\tilde{\tau}_1} < m_{\tilde{\chi}_1^\pm}$. For none of these points $\tilde{\chi}_2^0$ or $\tilde{\chi}_1^\pm$ have a significant branching fraction into slepton/lepton pairs. This has important consequences for collider searches, as we will discuss in Section 7.

Let us briefly come back to the $\tan\beta$ dependence. We have argued above that $\tan\beta = 10$ has a larger parameter space than higher values, but otherwise results are very similar. This is illustrated in Fig. 8, which shows scan results as in Fig. 5 but for $\tan\beta = 50$. As can be seen, the only change is that points with low DD cross sections, corresponding to a low $m_{\tilde{\nu}_2}$, are removed. Indeed the scan points for $\tan\beta = 50$ that pass all constraints are just a subset of those for $\tan\beta = 10$. In the following we will therefore use the $\tan\beta = 10$ scan points.

4.1 Uncertainties in the DD limits

As the DD limit plays a crucial role in constraining the parameter space, it is important to consider the uncertainties involved in extracting the limit on $\sigma^{SI}_{\chi p}$ from experiments. One source of uncertainty is the assumed DM velocity distribution. In particular, there is a minimum velocity necessary to pass the energy threshold of the detector, $v^2_{min} = \frac{m_N E_R}{2\mu^2_\chi}$. Thus the direct detection limit for low masses is particularly sensitive to the upper part of the velocity distribution. To illustrate this effect, we assume an isothermal velocity distribution and allow for a 2σ variation of $v_0 = 220 \pm 20$km/s. We also vary the velocity above which DM will escape from the Galaxy in the range $500 < v_{esc} < 600$km/s [65].[2] The local dark matter density is another factor that possesses a large uncertainty, it is generally assumed to

[2]Several velocity distributions were considered in [66,67]. Varying the input parameters of the isothermal distribution as we do, reproduces most of the span of variation of the limits found in those studies.

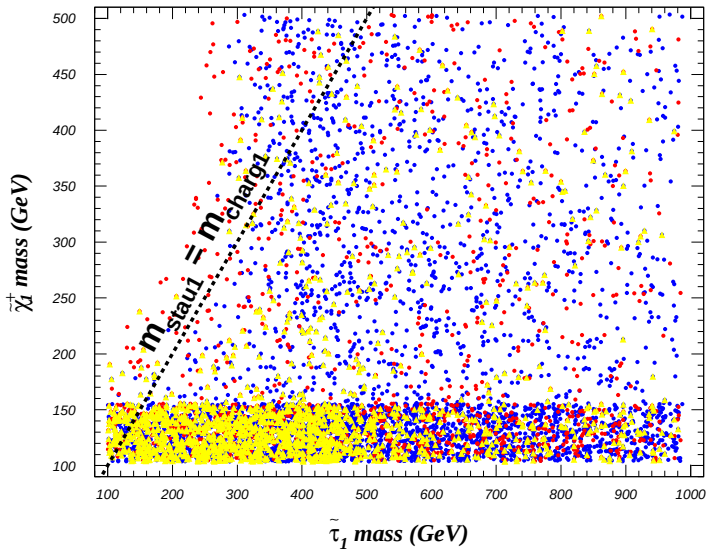

Figure 7: Same as the lhs plot of Fig. 5 but in the $m_{\tilde{\chi}_1^\pm}$ versus $m_{\tilde{\tau}_1}$ plane. The red (blue) dots denote points that have a relic density within (below) the 3σ WMAP range but too large a DD cross-section. The yellow triangles denote points that satisfy the WMAP upper bound as well as the DD limits from CoGeNT and Xenon10.

be $\rho = 0.3$ GeV/cm^3 but can vary from $0.2-0.7$. (For a review of astrophysical uncertainties on the velocity and density distribution see [68].)

Finally, there is an additional uncertainty that is specific to Xenon, it comes from the scintillation factor $L_{\rm eff}$ that allows to convert the measured electron energy into the nuclear recoil energy. In particular the threshold for nuclear recoil energy strongly depends on the scintillation factor at low energies. New measurements have shown that the scintillation efficiency can be significantly lower than the value used in Ref. [25]—and this especially at low energies—thus weakening the limit on $\sigma_{\chi p}^{SI}$ [69]. The Xenon10 limit in Fig. 6 uses a constant value for $L_{\rm eff}$ while the band for Xenon100 [26] uses a value of $L_{\rm eff}$ that decreases at low energies [70].

5 Results for three degenerate light sneutrinos

In the case of three light sneutrinos, the constraint from the Z width on the sneutrino mixing angle is stronger. Moreover, for three exactly degenerate sneutrinos, the relic density can increase by a factor up to 3 as compared to the one-generation case. This is because the effective annihilation cross-section including the coannihilation channels is $\langle \sigma v \rangle \propto (\sum g_i^2 \sigma_{ij})/\sum g_i^2$ where g_i is the number of degrees of freedom and σ_{ij} the cross-section for annihilation of two supersymmetric particles, χ_i, χ_j into SM particles. Thus when annihilation is dominated by the processes $\tilde{\nu}_i \tilde{\nu}_i^* \to f\bar{f}$, $\langle \sigma v \rangle$ increases by a factor of 3 as compared with the one generation case. This then leads to a tension between the relic density constraint which requires significant mixing and the Z width which strongly constrain this mixing angle. The relic density constraint is particularly severe at low masses where we had $\Omega h^2 \approx 0.11$ in the one generation case. The smaller mixing can of course be partially compensated by $A_{\tilde{\nu}}$ however this then typically violates the DD limits. Furthermore, for three light sneutrinos with large

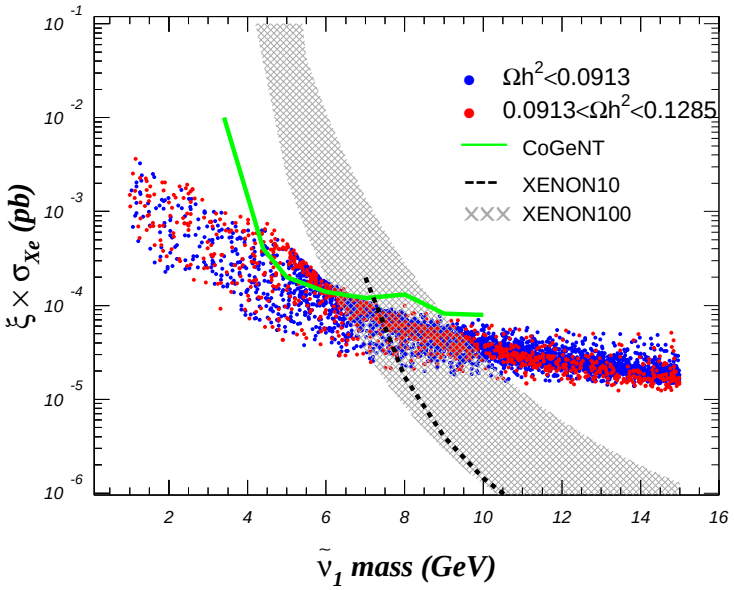

Figure 8: Same as Fig. 5 but for $\tan\beta = 50$.

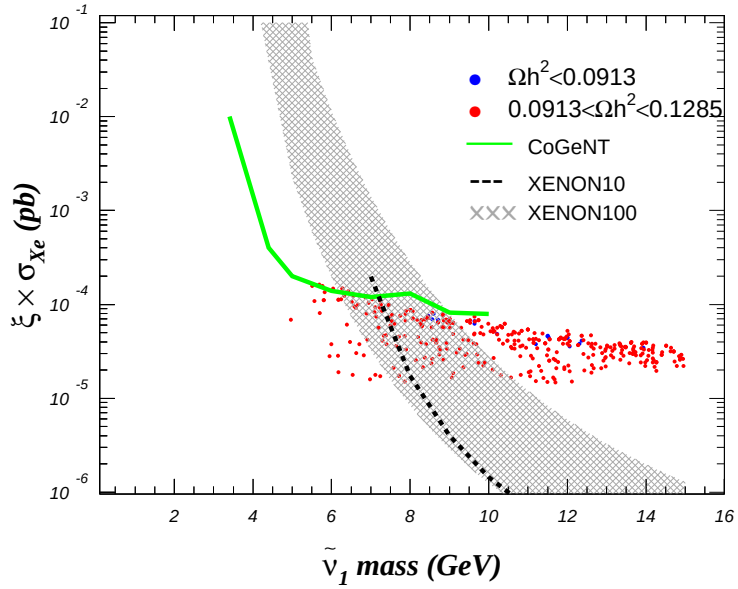

Figure 9: Scatter plot of $\sigma^{\rm SI}_{\tilde{\nu}_1 Xe}$ versus $m_{\tilde{\nu}_1}$ analogous to Fig. 6 but for three degenerate light sneutrinos.

$A_{\tilde{\nu}}$, the Higgs mass constraint becomes much more severe.

Decreasing M_2 makes it easier to satisfy the relic density constraint. Indeed in this case annihilation is dominated by production of neutrinos and all channels $\tilde{\nu}_i\tilde{\nu}_j \to \nu_i\nu_j$ contribute equally to the annihilation cross-section so that Ωh^2 is only a factor 3/2 larger than for the one generation case.

We perform a random scan analogous to the one in the previous section. The result of this scan is shown in Fig. 9. As expected, the parameter space for sneutrino DM is now much more restricted, and only few points pass all constraints. The allowed sneutrino masses now range from 4.5 to 8 GeV. For most scenarios the chargino mass lies just above the LEP limit.

The sneutrino mixing is around $\sin\theta_{\tilde{\nu}} \approx 0.27 - 0.29$, while the slepton masses are restricted to $m_{\tilde{\ell}_{L,R}} \approx m_{\tilde{\nu}_2} \approx 150 - 480$ GeV. This is because larger masses induce too large corrections to m_h, while smaller masses reduce the value of $A_{\tilde{\nu}}$ and thus the Higgs-exchange contribution to the annihilation processes. It is also interesting to note that in the DD-allowed region there are no points with Ωh^2 below the 3σ WMAP range (and overall there are only very few points with $\Omega h^2 < 0.0913$).

The exact mass splitting between sneutrinos of different flavours strongly influences the allowed parameter space. For example, a 1 GeV mass splitting is enough to suppress any coannihilation contributions to a negligible level. Such a mass splitting can be induced by small splittings in the soft terms, which are rather generic in supersymmetric models even if one starts out with universal soft terms at a high scale. Taking, for instance, $m_{\widetilde{L}_1} = m_{\widetilde{L}_2} = m_{\widetilde{L}_3}$, $m_{\widetilde{N}_1} = m_{\widetilde{N}_2} = m_{\widetilde{N}_3}$ and just 1% difference in the $A_{\tilde{\nu}}$ terms, $A_{\tilde{\nu}_{e,\mu}} = 0.99 A_{\tilde{\nu}_\tau}$, we find mass splittings of 2–14 GeV. In this case, the heavier $\tilde{\nu}_{1e,\mu}$ decay into the $\tilde{\nu}_{1\tau}$ LSP through 3-body modes [71] with decay widths ranging from 10^{-12} to 10^{-8} GeV. The dominant mode is into neutrinos; visible decays, e.g., $\tilde{\nu}_{1e} \to e^{\mp}\tau^{\pm}\tilde{\nu}_{1\tau}$, have at most few percent branching ratio. In this case we are back to the case of one light sneutrino presented previously with only a more severe constraint on $\sin\theta_{\tilde{\nu}}$ and $A_{\tilde{\nu}}$ from the Z width and light Higgs mass. In what follows we will therefore concentrate on the case of one light sneutrino.

6 Indirect detection

6.1 Neutrinos from annihilation in the Sun

Neutrinos originating from annihilation of DM captured in the Sun could provide a good signature for the mixed sneutrino model. In scenarios with light sneutrinos, a detector with a low threshold is needed. The Super-K detector has a threshold of 1.6 GeV, while large detectors like Antares or ICECUBE have threshold energies above 25 GeV, making them unsuitable for detecting the neutrino flux from light sneutrinos.

The capture rate for DM particles in the core of the Sun depends on the DM–nucleus scattering cross-section, as well as on the DM velocity distribution and local density. After being captured, the DM annihilates into Standard Model particles, which further decay into neutrinos that can be observed at the Earth. The capture rate is approximated as [72, 73]

$$\begin{aligned} C_{\tilde{\nu}_1} &= 4.8 \times 10^{24}\,\mathrm{s}^{-1} \left(\frac{\rho_{\tilde{\nu}_1}}{0.3\,\mathrm{GeV/cm}^3}\right)\left(\frac{270\,\mathrm{km/s}}{\bar{v}}\right) \\ &\quad \times \sum_i \left(\frac{\sigma^{\mathrm{SI}}_{\tilde{\nu}_1 i}}{10^{-40}\,\mathrm{cm}^2}\right)\frac{f_i \phi_i}{m_{\tilde{\nu}_1} m_{N_i}} F_i(m_{\tilde{\nu}_1}) S(m_{\tilde{\nu}_1}/m_{N_i}) \end{aligned}$$

where m_{N_i}, the mass of the nuclear species i, and $m_{\tilde{\nu}_1}$ are given in GeV. $\bar{v}$ is the DM velocity dispersion, f_i is the mass fraction of element i in the Sun, and ϕ_i its distribution. $F_i(m)$ is a form factor suppression and S a kinetic suppression factor. For these parameters, we use the values listed in Tables 8 and 9 of Ref. [72]. Finally, $\sigma^{\mathrm{SI}}_{\tilde{\nu}_1 i}$ is the elastic scattering cross-section on point-like nucleus.

In models where the DM is not self-conjugate, one can get different capture rates for particles and antiparticles. Furthermore both particle–particle (antiparticle–antiparticle) and particle–antiparticle annihilation channels exist, in our case $\tilde{\nu}_1\tilde{\nu}_1 \to \nu\nu$ ($A_{\chi\chi}$) and $\tilde{\nu}_1\tilde{\nu}_1^* \to$

$X\bar{X}$ ($A_{\chi\bar{\chi}}$). The equations describing the evolution of the number of DM (anti-)particles, $N_\chi(N_{\bar{\chi}})$, are then

$$\begin{aligned}\dot{N}_\chi &= C_\chi - 2A_{\chi\chi}N_\chi^2 - A_{\chi\bar{\chi}}N_\chi N_{\bar{\chi}}\,,\\ \dot{N}_{\bar{\chi}} &= C_{\bar{\chi}} - 2A_{\bar{\chi}\bar{\chi}}N_{\bar{\chi}}^2 - A_{\chi\bar{\chi}}N_\chi N_{\bar{\chi}}\,,\end{aligned} \tag{16}$$

The annihilation rates can be approximated as

$$A_{\chi\chi(\chi\bar{\chi})} = \frac{\langle\sigma v\rangle_{\chi\chi(\chi\bar{\chi})}}{V_{eff}}\,, \tag{17}$$

where $V_{eff} = 5.8\times10^{30}\mathrm{cm}^3(m_\chi/\mathrm{GeV})^{-3/2}$ is the effective volume of the core of the Sun [74]. If the capture and annihilation rates are sufficiently large, equilibrium is reached and the annihilation rate is only determined by the capture rate. We assume this to be the case. To take into account the different capture and annihilation rates for particles and antiparticles, we define

$$\beta = \frac{C_\chi}{C_{\bar{\chi}}}\,,\quad \alpha = \frac{A_{\chi\chi}}{A_{\chi\bar{\chi}}} = \frac{A_{\bar{\chi}\bar{\chi}}}{A_{\chi\bar{\chi}}}\,,\quad x = \frac{N_\chi}{N_{\bar{\chi}}}\,. \tag{18}$$

Then, after equilibrium is reached, $\dot{N}_\chi = \dot{N}_{\bar{\chi}} = 0$ and we can solve Eq. 16. The annihilation rate at present is determined by the capture rates as well as α:

$$\begin{aligned}\Gamma_{\chi\bar{\chi}} &= A_{\chi\bar{\chi}}N_\chi N_{\bar{\chi}} = \frac{C_{\bar{\chi}}}{1+\alpha x}\,,\\ \Gamma_{\chi\chi} &= A_{\chi\chi}N_\chi N_\chi = \frac{1}{2}C_\chi\left(\beta - \frac{1}{1+\alpha x}\right)\,,\\ \Gamma_{\bar{\chi}\bar{\chi}} &= A_{\bar{\chi}\bar{\chi}}N_{\bar{\chi}}N_{\bar{\chi}} = \frac{1}{2}C_{\bar{\chi}}\frac{\alpha x}{1+\alpha x}\,,\end{aligned} \tag{19}$$

where

$$x = \frac{1}{2\alpha\beta}\left[1-\beta+\left((\beta-1)^2+4\alpha^3\beta\right)^{1/2}\right]\,. \tag{20}$$

The total neutrino spectrum at the Earth, assuming self-annihilation channels are solely into neutrino pairs, is given by

$$\begin{aligned}\frac{d\phi_\nu}{dE_\nu} &= \frac{1}{4\pi d^2}\left(\Gamma_{\chi\chi}Br_{\nu\nu}\frac{dN_{\nu\nu}}{dE} + \Gamma_{\chi\bar{\chi}}\sum_f Br_{f\bar{f}}\frac{dN_f}{dE}\right)\,,\\ \frac{d\phi_{\bar{\nu}}}{dE_{\bar{\nu}}} &= \frac{1}{4\pi d^2}\left(\Gamma_{\bar{\chi}\bar{\chi}}Br_{\bar{\nu}\bar{\nu}}\frac{dN_{\bar{\nu}\bar{\nu}}}{dE} + \Gamma_{\chi\bar{\chi}}\sum_f Br_{f\bar{f}}\frac{dN_f}{dE}\right)\,,\end{aligned} \tag{21}$$

where $d = 1.5\times10^8$ km is the distance from the Sun to the Earth, $Br_{\nu\nu}$ is the branching fraction for annihilation into neutrino pairs $Br_{f\bar{f}}$ the branching fraction into each particle/antiparticle final state $f\bar{f}$. N_f and $N_{\nu\nu}(N_{\bar{\nu}\bar{\nu}})$ are the neutrino spectra resulting from those annihilations. Here $dN_{\nu\nu}/dE$ is simply proportional to a delta function. The neutrino spectrum originating from different annihilation channels into SM particles and taking into account oscillations was computed in [75], we use the tables given there. Note that for the neutrino pair an average over the three flavours in the annihilation process is assumed. For

the one light sneutrino scenario this is not the case, however this is still a good approximation since almost perfect 3-generation mixing is expected for neutrinos below 10 GeV propagating in the Sun [75].

For light DM particles, the process of evaporation from the Sun can be important, this effect was estimated in [73, 74]. We modify Eq. 16 accordingly and solve it iteratively. We find that for the range of annihilation cross-sections of our scenarios, the evaporation affects significantly DM particles lighter than 3 GeV and is irrelevant for heavier DM particles.

Finally, to compare with the data, one must compute the muon flux for upward events [76]

$$\frac{d\phi_\mu}{dE_\mu} = \int_0^{m_{\tilde{\nu}_1}} dE_\nu \frac{d\phi_\nu}{dE_\nu} \int_0^\infty dz \int_0^{E_\nu} dE_\mu^{'} \frac{dP_{cc}(E_\nu, E_\mu^{'})}{dz dE_\mu^{'}} P_{surv}(E_\mu^{'}, E_\mu)\delta(E_\mu - E_\mu(E_\mu^{'}, z)) \tag{22}$$

where the survival probability for a muon of energy E'_μ and final energy E_μ

$$P_{surv}(E_\mu^{'}, E_\mu) = \left(\frac{E_\mu}{E_\mu^{'}}\right)^y \left(\frac{\alpha + \beta E_\mu^{'}}{\alpha + \beta E_\mu}\right)^y \tag{23}$$

and the muon energy lost after propagating a distance z is

$$E_\mu(E_\mu^{'}, z) = e^{-\beta\rho z} E_\mu^{'} - \frac{\alpha}{\beta}(1 - e^{-\beta\rho z}) \tag{24}$$

Here $y = m_\mu/(c\tau\alpha\rho)$, τ is the muon lifetime, $\rho = 2.6$ g/cm^3 the rock density and $\alpha = 2 \times 10^{-3}$ GeV cm^2/g, $\beta = 3 \times 10^{-6}$ cm^2/g characterize the average energy loss of the muon traveling through rock or water. dP_{CC} is the probability for a neutrino with energy E_ν to be converted into a muon of energy E_μ over a distance dz through charged current interactions.

The event rate takes into account the effective area of the detector. For Super-K, the detector is cylindrical with a radius $R = 18.9$ m and a height 36.2 m. The muons that are stopped in the first 7 m are not observed, this corresponds to the muon energy threshold of $E = 1.6$ GeV. Furthermore, only muons of energy larger than 7.7 GeV go through the detector. This means that for our allowed scenarios with DM masses below 8 GeV, almost all the muons will be stopped within the detector. We therefore compute the rate for stopped muons only. To do this we take into account the zenith angle θ_z when computing the effective area of the detector and average over $-1 < \cos\theta < 0$ [77].

In Fig. 10, we display the total muon/antimuon rate as a function of the $\tilde{\nu}_1$ mass for the scan results of Section 4 (only the points that pass all constraints are used). The Super-K limit as extrapolated from [78] is also displayed. Here we take $\bar{v} = 270$ km/s for the DM velocity dispersion and $\rho_{\tilde{\nu}_1} = \xi \times 0.3$ GeV/cm^3 with the same re-scaling factor ξ as in Section 4 when the sneutrinos do not make up all the DM. Furthermore, we take the values of Eq. (13) for the quark coefficients. The larger rates are found for sneutrinos lighter than m_b that annihilate dominantly into $\tau^+\tau^-$ or neutrino pairs, since these modes give a harder neutrino spectrum. Some of our scenarios are within 10% of the experimental limit in the mass range $3-4$ GeV. In general, the expected rates are within one order of magnitude of the Super-K limit, except for $m_{\tilde{\nu}_1} < 3$ GeV where the evaporation effect becomes very important so that the neutrino flux is strongly suppressed. Note that these predictions depend on the DM velocity and average density. In particular a lower $\bar{v}$ would lead to larger neutrino rates. At the same time a lower DM velocity would relax the DD constraints.

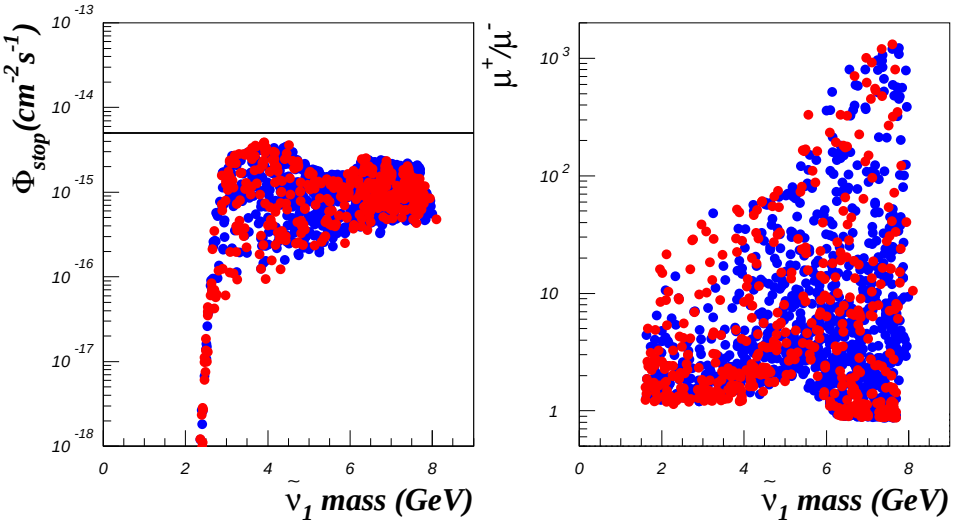

Figure 10: Predicted flux from stopped muons from the Sun in the Super-K detector for $\bar{v} = 270$ km/s (left) and the corresponding ratio of antimuon to muon fluxes (right), for the allowed scan points of Section 4, cf. Figs. 5 and 6. The red (blue) points have a relic density within (below) the 3σ WMAP range. The horizontal line in the lhs plot shows the extrapolated Super-K limit.

As already mentioned, one characteristic of our mixed sneutrino DM scenario is that the scattering rates on nucleons can differ significantly for particles and antiparticles. In fact, the capture of $\tilde{\nu}^*$ is in general more efficient than that of $\tilde{\nu}$ due to the destructive interference between the Z and Higgs exchanges in the latter case. As a result, the flux for antineutrinos and thus of antimuons is often much larger than that for muons, see the rhs plot in Fig. 10. Distinguishing muon from antimuon events would therefore provide an additional test of this model.

6.2 Photons

As mentioned previously, when $m_{\tilde{\nu}_1} \gtrsim 5$ GeV the dominant $\tilde{\nu}_1$ pair annihilation channels are $\nu_\tau\nu_\tau$ or $b\bar{b}$, while for lighter DM the charged fermion channels are $c\bar{c}$ and $\tau^+\tau^-$, with both channels having similar rates. Below ca. 1.5 GeV, the annihilation is purely into neutrinos. The annihilation channels into charged fermions leave a signature in photons, antiprotons and positrons. Photons are particularly interesting as the Fermi-LAT satellite is currently taking data in this channel. (The signature in charged cosmic rays is discussed in the next subsection.) The Fermi-LAT collaboration has obtained its first limits on the flux of photons originating from DM annihilations. In particular limits on σv were extracted from observations of dwarf galaxies [79]. The best one is obtained from Ursa Minor and corresponds to $\sigma v > 7 \times 10^{-26}\,\mathrm{cm}^3\,\mathrm{s}^{-1}$ for $m_{\mathrm{DM}} = 10$ GeV assuming an annihilation entirely into $b\bar{b}$.

To study the sensitivity to light sneutrino DM, we compute the annihilation cross-section into the $f\bar{f}$ channel, $\sigma v_{f\bar{f}}$, for the parameter points of Section 4 that pass all constraints. To this aim we assume a NFW dark matter profile [80]. The results are shown in Fig. 11 for

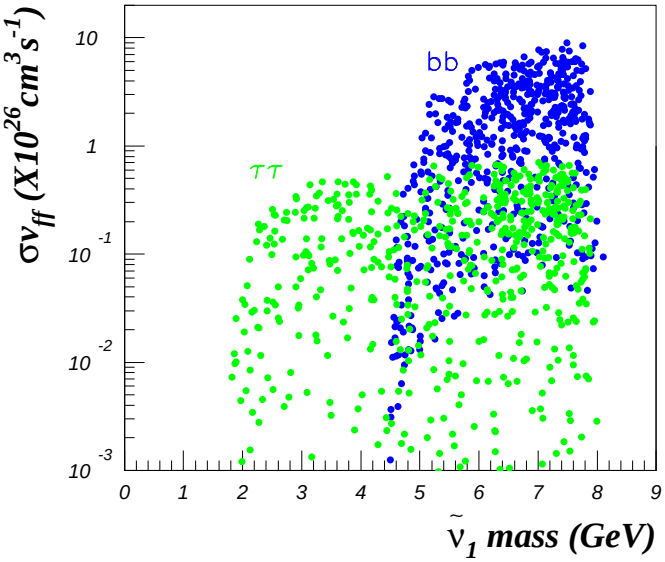

Figure 11: Annihilation cross-sections $\sigma v_{f\bar{f}}$ for $f = b$, τ as a function of $m_{\tilde{\nu}_1}$, for the allowed scenarios of Section 4.

$f = b$ and τ. The $c\bar{c}$ channel gives similar results to $\tau^+\tau^-$.

When $b\bar{b}$ is the dominant charged particle final state, $\sigma v_{b\bar{b}}$ ranges from $10^{-27}\,\mathrm{cm}^3\,\mathrm{s}^{-1}$ to $10^{-25}\,\mathrm{cm}^3\,\mathrm{s}^{-1}$. We therefore expect that some of our scenarios could be probed by Fermi-LAT once the analysis is extended to lower masses. When $\tau^+\tau^-$ is the dominant channel, $\sigma v_{\tau\bar{\tau}}$ can reach up to $10^{-26}\,\mathrm{cm}^3\,\mathrm{s}^{-1}$. However, this channel gives a harder photon spectrum, so that the sensitivity on the photon flux is expected to be almost an order of magnitude better than for the $b\bar{b}$ channel [79]. The Fermi-LAT satellite could therefore also probe some of the scenarios with $\tilde{\nu}_1$ masses below ca. 5 GeV. Note that for $m_{\tilde{\nu}_1} \lesssim 2$ GeV, the annihilation is dominated by neutrinos, leaving no signature in the photon channel. These scenarios are also the ones that because of evaporation have very suppressed rates in neutrino telescopes.

6.3 Charged particles: positrons and antiprotons

The annihilation into charged particles will also leave a signature for antiprotons and positrons. The flux of antiprotons has been measured by PAMELA [81] together with the ratio of antiprotons to protons. It is well described by the expected background flux from standard astrophysical processes, the spallation of cosmic ray proton and helium nuclei over the interstellar medium. There are, however, large uncertainties in the theoretical predictions of the secondary fluxes, due to uncertainties in the $\bar{p}$ production cross-sections, as well as in the parameters of the propagation models [82]. Each of these uncertainties have been estimated to be around 25% for the diffusion model with convection and re-acceleration described in [82]. Therefore there is still room for an additional contribution from DM annihilation, especially in the lower part of the spectrum where the experimental uncertainties are the largest. For an energy of $E_{\bar{p}} = 0.56$ GeV, for instance, which roughly corresponds to the peak of the spectrum from a 5 GeV DM particle, the measured flux is $\Phi_{\bar{p}} = 15.3^{+7.5}_{-3.7} \pm 0.9 \times 10^{-7}\ (\mathrm{GeV\,cm^2\,s\,sr})^{-1}$. The left panel in Fig. 12 shows antiproton spectra originating from $\tilde{\nu}_1$ annihilation for $m_{\tilde{\nu}_1} = 1.4$, 3.9 and 7.5 GeV from left to right for either line-style. For each of these masses we have selected two scenarios corresponding

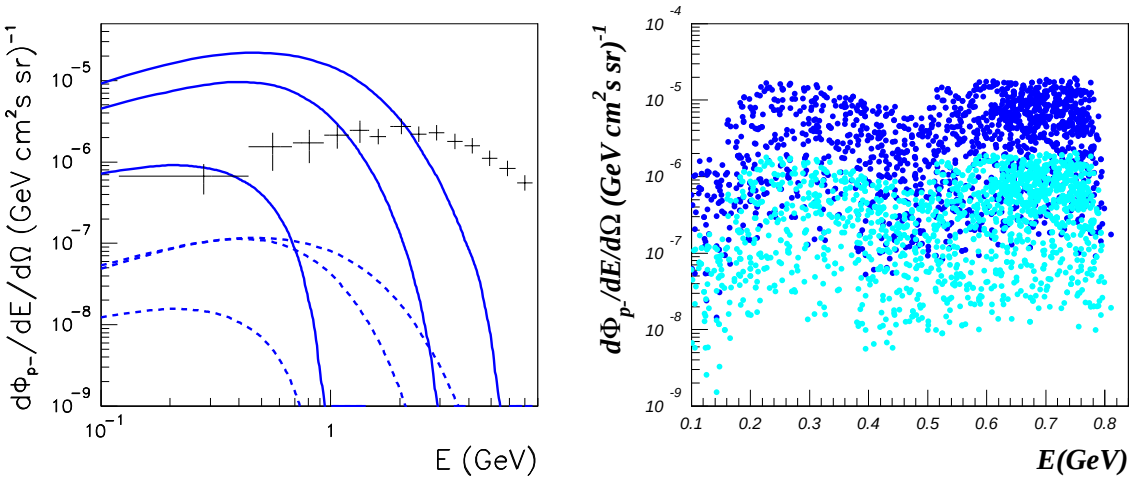

Figure 12: On the left, the antiproton spectrum for 6 representative allowed points as explained in the text; the antiproton flux measured by PAMELA [81] is also displayed (crosses). On the right, the differential flux for $\tilde{\nu}_1$ annihilation into antiprotons at $E = 0.1 m_{\tilde{\nu}_1}$ including propagation for two sets of propagation parameters, MIN (light blue points) and MED (dark blue points), see Table 1.

to near maximal (full lines) and near minimal (dashed lines) flux. The selected scenarios are within 10% of the absolute maximum/minimum fluxes. As can be seen, the predictions can vary by around two orders of magnitude for a given mass, depending on the details of the parameter point. Indeed, while the antiproton fluxes from $\tilde{\nu}_1$ annihilation alone can by far exceed the observed values in certain cases, they can also be more than one order of magnitude below the measurements and the expectations for the secondary spectrum.

The spectra we just discussed were obtained using the MED set of diffusion parameters as given in Table 1, together with a solar modulation in the force field approximation with $\phi_F = 250$ MeV [51]. These diffusion parameters are in fact source of an important uncertainty in the flux. For illustration, the plot on the right in Fig. 12 compares the antiproton flux at $E = 0.1 m_{\tilde{\nu}_1}$ obtained with the MED diffusion model (dark blue points) to that obtained with the MIN model (light blue points). The scattered points are the allowed scan points of the one-sneutrino case, and $E = 0.1 m_{\tilde{\nu}_1}$ was chosen because as the antiproton spectrum has its maximum at an energy that roughly corresponds to 10–15% of the DM mass. The plot gives an estimate of the strong dependence of the primary flux on the propagation parameters of nearly one order of magnitude just between the MIN and MED model. Similarly, it is possible to choose other propagation models (for example the MAX model) that further increase the flux by almost an order of magnitude. From Fig. 12 we see that most of our scenarios are below the 1σ uncertainties of the measured flux when assuming the MIN propagation model, while strong constraints on our scenarios are expected assuming the MED propagation model.[3]

Let us now turn to the positron fluxes. These are displayed in Fig. 13, again assuming the MIN and MED propagation models and $E = m_{\tilde{\nu}_1}/10$. Here the MIN model gives a flux from $\tilde{\nu}_1$ annihilation that is roughly a factor 1.5 higher than that obtained with the MED model. PAMELA has measured the positrons to electron ratio [85] but has not yet released the positron fluxes. We can compare however with the secondary flux computed

[3] A detailed fit to the antiprotons and $\bar{p}/p$ flux ratio will appear elsewhere.

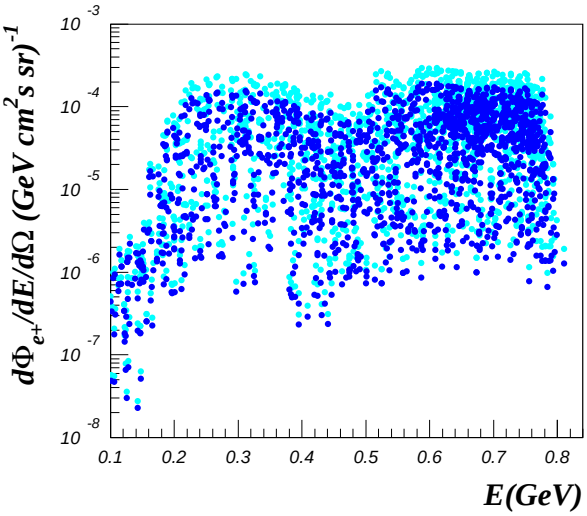

Figure 13: Differential flux for $\tilde{\nu}_1$ annihilation into positrons at $E = 0.1 m_{\tilde{\nu}_1}$ including propagation for two sets of propagation parameters, MIN (light blue points) and MED (dark blue points), see Table 1.

Model	δ	K_0 (kpc^2/Myr)	L (kpc)	V_C (km/s)
MIN	0.85	0.0016	1	13.5
MED	0.7	0.0112	4	12
MAX	0.46	0.0765	15	5

Table 1: Typical diffusion parameters that are compatible with the B/C analysis [83, 84].

in [86] which lies around $\Phi_{e^+} \approx 5 \times 10^{-4}\,(\mathrm{GeV\,cm^2\,s\,sr})^{-1}$ for the MED propagation model in the energy range $E = 0.2 - 0.8$ GeV relevant for our scenarios; for the MIN model, the predictions can increase by roughly a factor 2. From Fig. 13 we see that the positron flux from $\tilde{\nu}_1$ DM annihilation reaches at most $\Phi_{e^+} \approx 2\,(3) \times 10^{-4}\,(\mathrm{GeV\,cm^2\,s\,sr})^{-1}$ in the MED (MIN) model and hence is always smaller than the secondary flux.

7 Collider signatures of sneutrino DM

7.1 LHC

An important characteristic of the light sneutrino DM scenario is the invisible decay of the light Higgs [5]. At the LHC, the search for an invisible Higgs will be performed in the WW fusion channel with a signature in 2 tagged jets and missing E_T. Defining the ratio $\zeta^2 = \sigma(Hjj)/\sigma(hjj)_{SM} \times Br(h \to \mathrm{inv})$, the region to be probed with $\mathcal{L} = 10$ fb^{-1} at $\sqrt{s} = 14$ TeV corresponds to $\zeta^2 > 0.38$ for a Higgs mass below 150 GeV [87]. In our sneutrino DM scenarios, the light Higgs is SM-like and the invisible decay $h \to \tilde{\nu}_1 \tilde{\nu}_1^*$ overwhelmingly dominant ($\approx 99\%$), making for a good Higgs discovery potential in the invisible channel.

The SUSY signatures also differ from the expectations in the conventional MSSM: while squarks and gluinos have the usual cascade decays through charginos and neutralinos, with the same branching ratios as in the corresponding MSSM case (see, e.g., [88, 89]), here the

charginos and neutralinos decay further into the $\tilde{\nu}_1$ LSP. For 90% of the allowed parameter points of our scans, both the $\tilde{\chi}_1^0$ and the $\tilde{\chi}_2^0$ decay to practically 100% into $\nu\tilde{\nu}_1$, leading to larger missing E_T than naively expected for a LSP that weighs only a few GeV. (The $\tilde{\chi}_1^0$ in fact always decays invisibly.) Note also that in this case $\tilde{q}_R \to q\tilde{\chi}_1^0$ and $\tilde{q}_L \to q\tilde{\chi}_2^0$ give the same signature of jet+$E_T^{\rm miss}$, differing only in the jet-p_T and $E_T^{\rm miss}$ distributions. The $\tilde{\chi}_1^\pm$ also decays directly into the LSP, with BR($\tilde{\chi}_1^\pm \to l^\pm\tilde{\nu}_1$) $\approx$ 100% in the large majority of the cases. This means that decay chains involving charginos should on average have less missing E_T than chains involving neutralinos. It also means that $\tilde{\chi}_2^0\tilde{\chi}_1^\pm$ production leads to a single charged lepton rather than the usual trilepton signature. Furthermore if, as we have assumed, the LSP is the tau-sneutrino, the charged lepton will be a tau.

This picture depends only little on most of the parameters that we have fixed in the scans, in particular the value of the higgsino mass parameter μ hardly influences the picture (lowering μ increases a bit the $\tilde{\chi}_1^\pm \to W^\pm\tilde{\chi}_1^0$ decays, but these add to the single lepton events, although in a flavour-democratic way). The situation is, however, different for the first and second generation slepton masses: lowering them far enough can open up the $\tilde{\chi}_2^0 \to \ell^\pm\tilde{\ell}_L^\mp$ and/or $\tilde{\chi}_1^0 \to \ell^\pm\tilde{\ell}_R^\mp$ decay channels ($\ell = e, \mu$), and this crucially influences the experimental signatures. Setting, for instance, $m_{\tilde{L}_{1,2}} = m_{\tilde{R}_{1,2}} = 100$ GeV in the DM allowed scan points, while assuming that the RH $\tilde{\nu}_{e,\mu}$ are heavy, gives $\tilde{\chi}_2^0 \to \ell^\pm\tilde{\ell}_L^\mp$ decay branching ratios of typically up to 30%, and up to 50% if the decay into $\nu_\tau\tilde{\nu}_{1\tau}$ is suppressed by a small mixing angle (the rest goes into LH $\tilde{\nu}_{e,\mu}$'s). Note that decays into staus are mostly absent in this case. Taking, as may seem more natural, $m_{\tilde{L}_1} = m_{\tilde{L}_2} \approx m_{\tilde{L}_3}$, $m_{\tilde{N}_1} = m_{\tilde{N}_2} \approx m_{\tilde{N}_3}$ and $|A_{\tilde{\nu}_{e,\mu}}| \lesssim |A_{\tilde{\nu}_\tau}|$ brings us back to the situation that invisible neutralino decays are overwhelmingly dominant. The $\tilde{\chi}_1^\pm$ decays democratically into all three lepton flavours in this case, $\tilde{\chi}_1^\pm \to l^\pm\tilde{\nu}_{1l}$, with only a small preference for $\tau^\pm\tilde{\nu}_{1\tau}$. Finally, for $A_{\tilde{\nu}_{e,\mu}} \to 0$ we recover the situation discussed in the previous paragraph, with $\tilde{\chi}_2^0 \to \nu_\tau\tilde{\nu}_{1\tau}$ and $\tilde{\chi}_1^\pm \to \tau^\pm\tilde{\nu}_{1\tau}$ having practically 100% branching ratio.

A detailed study of the LHC potential to resolve the light sneutrino DM scenario, including in particular the determination of the DM mass from $\tilde{q} \to q'\tilde{\chi}_1^\pm \to q'l^\pm\tilde{\nu}_{1l}$ events, is left for future work.

7.2 ILC signatures

At an international linear collider (ILC) with $\sqrt{s} = 500$ GeV, the main production for the light Higgs is $e^+e^- \to Zh$. This allows for precision measurements even if the h decays entirely via invisible modes as is the case in our model [90]. The main SUSY production processes at the ILC are $\tilde{\chi}_1^\pm\tilde{\chi}_1^\mp, \tilde{\chi}_1^0\tilde{\chi}_2^0, \tilde{\chi}_2^0\tilde{\chi}_2^0, \tilde{\nu}_1\tilde{\nu}_1^*$ as well as $\tilde{\tau}_1^+\tilde{\tau}_1^-$ (and maybe selectrons and smuons, depending on the scenario).

Chargino-pair production has the largest cross-section and should be easily measurable, as is illustrated in Fig. 14. The peculiarity of the sneutrino DM model is that the chargino decay gives a single charged lepton plus missing energy, see the discussion in the previous subsection. The cross-section for stau-pair production can reach 70 fb if the staus are kinematically accessible. This occurs, however, only for a small fraction of the successful DM models, cf. Fig. 7. The rather heavy staus in our scenarios are a consequence of setting $m_{\tilde{L}_3} = m_{\tilde{R}_3}$. This assumption was not important for the DM study but has a strong impact here. Furthermore, the assumption of heavy selectrons and smuons means that the most favourable production processes, notably $e^+e^- \to \tilde{e}^+\tilde{e}^-$ and $e^+e^- \to \tilde{\mu}^+\tilde{\mu}^-$, are kinematically not accessible. Relaxing this assumption, for example by assuming universality in the

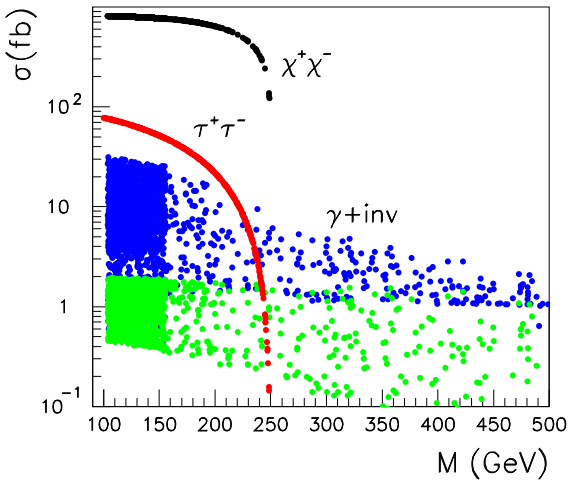

Figure 14: Scatter plot of the unpolarized cross-sections of $e^+e^- \to \tilde{\chi}_1^\pm \tilde{\chi}_1^\mp$ (black) and γ+inv (green) at $\sqrt{s} = 500$ GeV as a function of $m_{\tilde{\chi}_1^\pm}$, and of $e^+e^- \to \tilde{\tau}_1^+ \tilde{\tau}_1^-$ (red) as a function of $m_{\tilde{\tau}_1}$ for the allowed scenarios with one light sneutrino. Also shown is the single photon cross-section assuming $m_{\tilde{e}_R} = m_{\tilde{e}_L} = m_{\tilde{\tau}_R}$.

slepton masses, could give large selectron/smuon pair-production cross-sections and would also affect chargino-pair production, which depends on the mass of the LH $\tilde{\nu}_e$.

As mentioned, neutral particles have large branching fractions into invisible states. In fact, the $\tilde{\chi}_1^0, \tilde{\chi}_2^0 \to \tilde{\nu}_1 \nu$ decays both have nearly 100% branching fractions. Therefore, $\tilde{\nu}_1 \tilde{\nu}_1^*$ and $\tilde{\chi}_i^0 \tilde{\chi}_j^0$ $(i, j = 1, 2)$ pair production will all contribute to the single photon cross-section. We have computed the total single photon cross-section exactly using calcHEP [57] with the cuts $p_T^\gamma > 4$ GeV and $\theta_{beam\gamma} > 10°$. Monte Carlo simulations of this process including backgrounds have shown that cross sections around 1.6 fb could be detectable using beam polarisation [91, 92] [4]. For the allowed points from Section 4, the predictions for the unpolarised cross-section are mostly below 1 fb although the cross-section can reach up to 2 pb when $M_2 <$ 150 GeV, cf. the green points in Fig. 14. The dominant contribution arises from the $\tilde{\nu}_1 \tilde{\nu}_1^*$ channel. The mass of the selectron is again a crucial parameter for these processes. To illustrate its impact we have also computed the single photon cross-section fixing $m_{\tilde{e}_R} = m_{\tilde{e}_L} = m_{\tilde{\tau}_L} = m_{\tilde{\tau}_R}$ (instead of 1 TeV). This increases the single photon cross-section by up to one order of magnitude, see the blue points in Fig. 14. This is due mainly to the increase in neutralino production.

Note finally that although there can be an important additional Higgs production mode through the decay $\tilde{\nu}_2 \to \tilde{\nu}_1 h$, this is not detectable since the Higgs decays invisibly. Furthermore, in our model the $\tilde{\nu}_2$ is often too heavy to be pair produced with $\sqrt{s} = 500$ GeV.

8 Conclusions

In supersymmetric models with Dirac neutrino masses, a weak-scale trilinear $A_{\tilde{\nu}}$ term that is not proportional to the small neutrino Yukawa couplings can induce a sizable mixing

[4] More detailed analyses including detector simulation for the ILC were also performed for DM masses above 100 GeV [93,94], it remains to be seen how can this be applied to our model where particles of different masses contribute to the single photon channel.

between LH and RH sneutrinos and render the lighter sneutrino mass eigenstate a viable dark matter candidate. In particular, the mixed sneutrino can be an excellent candidate for light SUSY DM with mass below ∼10 GeV, as we have shown in this paper.

To obtain a very light $\tilde{\nu}_1$ requires some fine-tuning, as the soft-breaking terms in the sneutrino mass matrix are all of the weak scale. Moreover, a viable sneutrino DM candidate requires enough mixing to provide sufficient pair-annihilation, while on the other hand the mixing should not be too large in order not to exceed the DD limits or contribute too much to the Z invisible decay width. In addition, the 1-loop diagrams involving sneutrinos induce a negative correction to the light Higgs mass, which can attain a few GeV for large $A_{\tilde{\nu}}$. In a random scan over 10^5 points for the case of one light sneutrino contributing to the DM, we found close to 2000 points that survive all present constraints, including the Z invisible decay width, the Higgs and SUSY mass limits, as well as dark matter constraints from the relic abundance and the direct detection experiments. These points populate the region $m_{\tilde{\nu}_1} \approx 1 - 8$ GeV. We also found that for very light $\tilde{\nu}_1$ below ca. 5 GeV, small $M_2 \approx 100 - 150$ GeV is preferred in order to enhance $\tilde{\nu}_1\tilde{\nu}_1 \to \nu\nu$ annihilation through t-channel wino exchange. In the case of three degenerate light sneutrinos, the constrains are much stronger and only few points pass all constraints.

Our results for direct and indirect detection of light sneutrino DM can be summarized as follows. First, the cross-section for the spin-independent elastic scattering on nuclei is predicted to be $\sigma^{\rm SI} > 10^{-5}$ pb. That is at most within an order of magnitude of present limits for DM masses around 5–10 GeV, and it includes the region favoured by CoGeNT (and perhaps CRESST). Second, sneutrino pair annihilation into $b\bar{b}$ and $\tau^+\tau^-$ can lead to large distortions of the positron and antiproton spectra at low energies. These are being probed by PAMELA. Furthermore, the photon flux can be in the range being probed by FermiLAT, provided again the $\tilde{\nu}_1$'s annihilate significantly into $b\bar{b}$ and $\tau^+\tau^-$. In all cases the signals are expected in the low energy range (ca. $0.1 - 3$ GeV), a region where measurements are not as precise as for higher energies. Third, the neutrino flux resulting from $\tilde{\nu}_1$ capture in the Sun can also be large. However, because the energy of the neutrinos is bounded by the DM mass, these scenarios are harder to probe than those with typical weak scale DM. In fact the neutrino energy is below the threshold of the large detectors. Only SuperKamiokande has a low enough threshold to have some sensitivity to neutrinos from light sneutrino annihilation, though these neutrinos do not have enough energy to induce muons that go through the detector. One can therefore use only events where muons are stopped in the detector. It is also interesting to note that the predicted flux for antineutrinos, and thus for antimuons, is often much larger than that for muons.

While the scenarios with $\tilde{\nu}_1$ DM that annihilates preferentially into $b\bar{b}$ have good prospects of being detected in the near future, those that have a DM mass below ca. 2 GeV will mostly escape detection. Indeed direct detection experiments lack sensitivity for these masses. Moreover, the main annihilation channel in this case is into neutrinos, leaving low chances for indirect detection in photons, antiprotons and positrons; some possibilities remain if the annihilation into $\tau^+\tau^-$ is significant. Even the neutrino telescopes cannot make use of the large branching fraction for annihilation into neutrinos, because the evaporation process in the Sun strongly suppresses the neutrino flux for such light $\tilde{\nu}_1$'s.

Finally a mixed sneutrino LSP leaves distinct signatures in collider experiments. Most notably the light Higgs boson and the two lightest neutralinos decay almost exclusively into invisible modes, while decays of the lighter chargino give a single charged lepton plus missing energy. At the LHC, the typical cascade decays therefore are $\tilde{q} \to q\tilde{\chi}_1^\pm \to q' l^\pm \tilde{\nu}_1$,

$\tilde{q}_L \to q\tilde{\chi}_2^0 \to q\nu\tilde{\nu}_1$ and $\tilde{q}_R \to q\tilde{\chi}_1^0 \to q\nu\tilde{\nu}_1$, all giving different amount of missing E_T. Moreover, $\tilde{\chi}_1^\pm\tilde{\chi}_2^0$ production gives only a single charged lepton. At the ILC, $\tilde{\nu}_1\tilde{\nu}_1^*$ and $\tilde{\chi}_i^0\tilde{\chi}_j^0$ $(i,j=1,2)$ pair production will all contribute to the single photon cross-section.

The details of the DM signatures at colliders depend of course on the assumptions that are made on the rest of the spectrum, in particular the first and second generation of sleptons. The predictions in astroparticle experiments have uncertainties from astrophysical and nuclear parameters. These include uncertainties in the quark content of the nucleon, on the local dark matter density and velocity distribution, on the dark matter halo profile and, for charged cosmic rays, on the parameters of the propagation model.

Last but not least if signals are found in astroparticle and collider experiments, the challenge will be to determine the precise DM properties and the underlying new physics. This requires in particular collider measurements of the masses and couplings of the DM and other new particles associated with it in order to refine and test the theoretical predictions for astroparticle observables. Moreover, if an $E_T^{\rm miss}$ signal is seen at the LHC, it should be confirmed in direct DM detection and vice versa, the agreement of the DM mass and cross-section determined in the two ways being a crucial test. To this end it will be interesting to investigate how well our light sneutrino DM scenarios can be resolved at the LHC by exploiting the $\tilde{q} \to q\tilde{\chi}_1^\pm \to q' l^\pm \tilde{\nu}_1$ cascade decay. Such a signature has been suggested in [95] as a method of measuring mass differences in the MSSM. This will be a future work.

9 Acknowledgments

We thank M. Cirelli, J. Collar, E. Nuss and T. Schwetz for useful discussions. EKP acknowledges the hospitality of LAPTH, LPSC and CERN, where most of this work was performed. This work is supported by HEPTOOLS under contract MRTN-CT-2006-035505. This work is also supported in part by the GDRI-ACPP of CNRS and by the French ANR project `ToolsDMColl`, BLAN07-2-194882. The work of AP is supported by the Russian foundation for Basic Research, grant RFBR-08-02-00856-a, RFBR-08-02-92499-a and RFBR-10-02-01443-a.

A Vertices involving sneutrinos

The Feynman rules of relevant $\tilde{\nu}_1$ couplings include

$$\begin{aligned}
Z^\mu\tilde{\nu}_1^*(p')\tilde{\nu}_1(p): &\quad -i\frac{e}{\sin 2\theta_W}(p+p')^\mu \sin\theta_{\tilde{\nu}}^2\,,\\
h\tilde{\nu}_2^*\tilde{\nu}_1: &\quad -iem_Z\frac{\sin(\alpha+\beta)}{\sin 2\theta_W}\cos\theta_{\tilde{\nu}}\sin\theta_{\tilde{\nu}} - i\frac{1}{\sqrt{2}}A_{\tilde{\nu}}\cos\alpha(\cos^2\theta_{\tilde{\nu}}-\sin^2\theta_{\tilde{\nu}})\,,\\
h\tilde{\nu}_1^*\tilde{\nu}_1: &\quad iem_Z\frac{\sin(\alpha+\beta)}{\sin 2\theta_W}\sin^2\theta_{\tilde{\nu}} + i\sqrt{2}A_{\tilde{\nu}}\cos\alpha\cos\theta_{\tilde{\nu}}\sin\theta_{\tilde{\nu}}\,.
\end{aligned} \tag{25}$$

$$
\begin{aligned}
W^\mu \tilde{\nu}_1 \tilde{l}_i \quad &: \quad i\frac{g}{\sqrt{2}} Z^l_{i1} (p+p')^\mu \sin\theta_{\tilde{\nu}} \\
\tilde{\chi}^0_i \tilde{\nu}^*_1 \nu \quad &: \quad -i\frac{g}{2\sqrt{2}\sin 2\theta_W} (c_W N_{i2} - s_W N_{i1}) \sin\theta_{\tilde{\nu}} (1+\gamma_5) \\
\tilde{\chi}^+_i \tilde{\nu}^*_1 l \quad &: \quad -i\frac{g}{4 m_W \cos\beta} \left[2 m_W \cos\beta V_{1i} (1-\gamma_5) - \sqrt{2} M_l U_{2i} (1+\gamma_5) \right] \sin\theta_{\tilde{\nu}}
\end{aligned}
\tag{26}
$$

Here Z^l is the charged lepton mixing matrix that is diagonal in flavour space, N is the neutralino mixing matrix and U, V the chargino mixing matrices. We use the SLHA notation for the MSSM part of the Lagrangian [96].

References

[1] B. Pontecorvo, *Neutrino experiments and the question of leptonic-charge conservation*, *Sov. Phys. JETP* **26** (1968) 984–988.

[2] V. N. Gribov and B. Pontecorvo, *Neutrino astronomy and lepton charge*, *Phys. Lett.* **B28** (1969) 493.

[3] S. M. Bilenky, C. Giunti, and W. Grimus, *Phenomenology of neutrino oscillations*, *Prog. Part. Nucl. Phys.* **43** (1999) 1–86, [hep-ph/9812360].

[4] M. C. Gonzalez-Garcia and M. Maltoni, *Phenomenology with Massive Neutrinos*, *Phys. Rept.* **460** (2008) 1–129, [arXiv:0704.1800].

[5] N. Arkani-Hamed, L. J. Hall, H. Murayama, D. Tucker-Smith, and N. Weiner, *Small neutrino masses from supersymmetry breaking*, *Phys. Rev.* **D64** (2001) 115011, [hep-ph/0006312].

[6] **WMAP** Collaboration, J. Dunkley *et al.*, *Five-Year Wilkinson Microwave Anisotropy Probe (WMAP) Observations: Likelihoods and Parameters from the WMAP data*, *Astrophys. J. Suppl.* **180** (2009) 306–329, [arXiv:0803.0586].

[7] E. Komatsu *et al.*, *Seven-Year Wilkinson Microwave Anisotropy Probe (WMAP) Observations: Cosmological Interpretation*, arXiv:1001.4538.

[8] N. Jarosik *et al.*, *Seven-Year Wilkinson Microwave Anisotropy Probe (WMAP) Observations: Sky Maps, Systematic Errors, and Basic Results*, arXiv:1001.4744.

[9] J. L. Feng, J. Kumar, J. Learned, and L. E. Strigari, *Testing the Dark Matter Interpretation of the DAMA/LIBRA Result with Super-Kamiokande*, *JCAP* **0901** (2009) 032, [arXiv:0808.4151].

[10] Y. G. Kim and S. Shin, *Singlet Fermionic Dark Matter explains DAMA signal*, *JHEP* **05** (2009) 036, [arXiv:0901.2609].

[11] D. G. Cerdeno and O. Seto, *Right-handed sneutrino dark matter in the NMSSM*, *JCAP* **0908** (2009) 032, [arXiv:0903.4677].

[12] A. L. Fitzpatrick, D. Hooper, and K. M. Zurek, *Implications of CoGeNT and DAMA for Light WIMP Dark Matter*, *Phys. Rev.* **D81** (2010) 115005, [arXiv:1003.0014].

[13] S. Andreas, C. Arina, T. Hambye, F.-S. Ling, and M. H. G. Tytgat, *A light scalar WIMP through the Higgs portal and CoGeNT*, arXiv:1003.2595.

[14] R. Essig, J. Kaplan, P. Schuster, and N. Toro, *On the Origin of Light Dark Matter Species*, arXiv:1004.0691.

[15] S. Chang, J. Liu, A. Pierce, N. Weiner, and I. Yavin, *CoGeNT Interpretations*, arXiv:1004.0697.

[16] K. J. Bae, H. D. Kim, and S. Shin, *Light neutralino dark matter with a very light Higgs for CoGeNT and DAMA/LIBRA data*, arXiv:1005.5131.

[17] Y. Mambrini, *The kinetic dark-mixing in the light of CoGENT and XENON100*, *JCAP* **1009** (2010) 022, arXiv:1006.3318.

[18] D. Das and U. Ellwanger, *Light dark matter in the NMSSM: upper bounds on direct detection cross sections*, arXiv:1007.1151.

[19] J. Lavalle, *10 GeV dark matter candidates and cosmic-ray antiprotons*, arXiv:1007.5253.

[20] **DAMA** Collaboration, R. Bernabei *et al.*, *First results from DAMA/LIBRA and the combined results with DAMA/NaI*, *Eur. Phys. J.* **C56** (2008) 333–355, [arXiv:0804.2741].

[21] **CoGeNT** Collaboration, C. E. Aalseth *et al.*, *Results from a Search for Light-Mass Dark Matter with a P- type Point Contact Germanium Detector*, arXiv:1002.4703.

[22] **The CDMS-II** Collaboration, Z. Ahmed *et al.*, *Results from the Final Exposure of the CDMS II Experiment*, arXiv:0912.3592.

[23] J. Kopp, T. Schwetz, and J. Zupan, *Global interpretation of direct Dark Matter searches after CDMS-II results*, *JCAP* **1002** (2010) 014, [arXiv:0912.4264].

[24] C. Savage, G. Gelmini, P. Gondolo, and K. Freese, *XENON10/100 dark matter constraints in comparison with CoGeNT and DAMA: examining the Leff dependence*, arXiv:1006.0972.

[25] **XENON** Collaboration, J. Angle *et al.*, *First Results from the XENON10 Dark Matter Experiment at the Gran Sasso National Laboratory*, *Phys. Rev. Lett.* **100** (2008) 021303, [arXiv:0706.0039].

[26] **XENON100** Collaboration, E. Aprile *et al.*, *First Dark Matter Results from the XENON100 Experiment*, arXiv:1005.0380.

[27] W. Seidel, "CRESST-II." Plenary talk at the 8th International Workshop on the Identification of Dark Matter (IDM10), 26-30 July 2010, Montpellier, France.

[28] G. Belanger, F. Boudjema, A. Cottrant, A. Pukhov, and S. Rosier-Lees, *Lower limit on the neutralino mass in the general MSSM*, *JHEP* **03** (2004) 012, [hep-ph/0310037].

[29] D. Feldman, Z. Liu, and P. Nath, *Low Mass Neutralino Dark Matter in the MSSM with Constraints from $B_s \to \mu^+\mu^-$ and Higgs Search Limits*, *Phys. Rev.* **D81** (2010) 117701, [arXiv:1003.0437].

[30] **CDF** Collaboration, T. Aaltonen *et al.*, *Search for $B_s^0 \to \mu^+\mu^-$ and $B_d^0 \to \mu^+\mu^-$ decays with $2fb^{-1}$ of $p\bar{p}$ collisions*, *Phys. Rev. Lett.* **100** (2008) 101802, [arXiv:0712.1708].

[31] D. A. Vasquez, G. Belanger, C. Boehm, A. Pukhov and J. Silk, *Can neutralinos in the MSSM and NMSSM scenarios still be light?*, arXiv:1009.4380 [hep-ph].

[32] C. Arina and N. Fornengo, *Sneutrino cold dark matter, a new analysis: Relic abundance and detection rates*, *JHEP* **11** (2007) 029, [arXiv:0709.4477].

[33] Z. Thomas, D. Tucker-Smith, and N. Weiner, *Mixed Sneutrinos, Dark Matter and the LHC*, *Phys. Rev.* **D77** (2008) 115015, [arXiv:0712.4146].

[34] L. J. Hall, T. Moroi, and H. Murayama, *Sneutrino cold dark matter with lepton-number violation*, *Phys. Lett.* **B424** (1998) 305–312, [hep-ph/9712515].

[35] S. Kolb, M. Hirsch, H. V. Klapdor-Kleingrothaus, and O. Panella, *Collider signatures of sneutrino cold dark matter*, *Phys. Lett.* **B478** (2000) 262–268, [hep-ph/9910542].

[36] T. Asaka, K. Ishiwata, and T. Moroi, *Right-handed sneutrino as cold dark matter*, *Phys. Rev.* **D73** (2006) 051301, [hep-ph/0512118].

[37] T. Asaka, K. Ishiwata, and T. Moroi, *Right-handed sneutrino as cold dark matter of the universe*, *Phys. Rev.* **D75** (2007) 065001, [hep-ph/0612211].

[38] H.-S. Lee, K. T. Matchev, and S. Nasri, *Revival of the thermal sneutrino dark matter*, *Phys. Rev.* **D76** (2007) 041302, [hep-ph/0702223].

[39] C. Arina, *Sneutrino cold dark matter in extended MSSM models*, arXiv:0805.1991.

[40] C. Arina, F. Bazzocchi, N. Fornengo, J. C. Romao, and J. W. F. Valle, *Minimal supergravity sneutrino dark matter and inverse seesaw neutrino masses*, *Phys. Rev. Lett.* **101** (2008) 161802, [arXiv:0806.3225].

[41] D. G. Cerdeno, C. Munoz, and O. Seto, *Right-handed sneutrino as thermal dark matter*, *Phys. Rev.* **D79** (2009) 023510, [arXiv:0807.3029].

[42] F. Deppisch and A. Pilaftsis, *Thermal right-handed sneutrino dark matter in the F_D-term model of hybrid inflation*, *JHEP* **0810** (2008) 080, [arXiv:0808.0490].

[43] R. Allahverdi, B. Dutta, K. Richardson-McDaniel, and Y. Santoso, *Sneutrino Dark Matter and the Observed Anomalies in Cosmic Rays*, *Phys. Lett.* **B677** (2009) 172–178, [arXiv:0902.3463].

[44] D. A. Demir, L. L. Everett, M. Frank, L. Selbuz, and I. Turan, *Sneutrino Dark Matter: Symmetry Protection and Cosmic Ray Anomalies*, *Phys. Rev.* **D81** (2010) 035019, [arXiv:0906.3540].

[45] R. Allahverdi, S. Bornhauser, B. Dutta, and K. Richardson-McDaniel, *Prospects for Indirect Detection of Sneutrino Dark Matter with IceCube*, *Phys. Rev.* **D80** (2009) 055026, [arXiv:0907.1486].

[46] D. G. Cerdeno, *Thermal right-handed sneutrino dark matter in the NMSSM*, *AIP Conf. Proc.* **1178** (2009) 16–22.

[47] R. Allahverdi, *Sneutrino dark matter in light of PAMELA*, arXiv:0909.5643.

[48] A. Kumar, D. Tucker-Smith, and N. Weiner, *Neutrino Mass, Sneutrino Dark Matter and Signals of Lepton Flavor Violation in the MRSSM*, arXiv:0910.2475.

[49] J. March-Russell, C. McCabe, and M. McCullough, *Neutrino-Flavoured Sneutrino Dark Matter*, *JHEP* **03** (2010) 108, [arXiv:0911.4489].

[50] G. Belanger, F. Boudjema, A. Pukhov, and A. Semenov, *Dark matter direct detection rate in a generic model with micrOMEGAs2.2*, *Comput. Phys. Commun.* **180** (2009) 747–767, [arXiv:0803.2360].

[51] G. Belanger *et al.*, *Indirect search for dark matter with micrOMEGAs2.4*, arXiv:1004.1092.

[52] A. Djouadi, J.-L. Kneur, and G. Moultaka, *SuSpect: A Fortran code for the supersymmetric and Higgs particle spectrum in the MSSM*, *Comput. Phys. Commun.* **176** (2007) 426–455, [hep-ph/0211331].

[53] D. M. Pierce, J. A. Bagger, K. T. Matchev, and R.-j. Zhang, *Precision corrections in the minimal supersymmetric standard model*, *Nucl. Phys.* **B491** (1997) 3–67, [hep-ph/9606211].

[54] **ALEPH, DELPHI, L3 and OPAL** Collaboration, LEP2 SUSY Working Group,. http://lepsusy.web.cern.ch/lepsusy/.

[55] **ALEPH, DELPHI, L3 and OPAL** Collaboration, LEP Working Group for Higgs Boson Searches, S. Schael, *et al.*, *Search for neutral MSSM Higgs bosons at LEP*, *Eur. Phys. J.* **C47** (2006) 547–587, [hep-ex/0602042].

[56] **L3** Collaboration, P. Achard *et al.*, *Single photon and multiphoton events with missing energy in e^+e^- collisions at LEP*, *Phys. Lett.* **B587** (2004) 16–32, [hep-ex/0402002].

[57] A. Pukhov, *Calchep 2.3: MSSM, structure functions, event generation, 1, and generation of matrix elements for other packages*, hep-ph/0412191.

[58] J. Goodman *et al.*, *Constraints on Light Majorana Dark Matter from Colliders*, arXiv:1005.1286.

[59] Y. Bai, P. J. Fox, and R. Harnik, *The Tevatron at the Frontier of Dark Matter Direct Detection*, arXiv:1005.3797.

[60] **CDF** Collaboration, T. Aaltonen *et al.*, *Search for large extra dimensions in final states containing one photon or jet and large missing transverse energy produced in $p\bar{p}$ collisions at $\sqrt{s}$ = 1.96-TeV*, *Phys. Rev. Lett.* **101** (2008) 181602, [arXiv:0807.3132].

[61] J. Gasser, H. Leutwyler, and M. E. Sainio, *Sigma term update*, *Phys. Lett.* **B253** (1991) 252–259.

[62] M. M. Pavan, I. I. Strakovsky, R. L. Workman, and R. A. Arndt, *The pion nucleon Sigma term is definitely large: Results from a GWU analysis of pi N scattering data*, *PiN Newslett.* **16** (2002) 110–115, [hep-ph/0111066].

[63] **JLQCD** Collaboration, H. Ohki *et al.*, *Calculation of the nucleon sigma term and strange quark content with two flavors of dynamical overlap fermions*, *PoS* **LATTICE2008** (2008) 126, [arXiv:0810.4223].

[64] R. Babich *et al.*, *Strange quark content of the nucleon*, *PoS* **LATTICE2008** (2008) 160, [arXiv:0901.4569].

[65] M. C. Smith *et al.*, *The RAVE Survey: Constraining the Local Galactic Escape Speed*, *Mon. Not. Roy. Astron. Soc.* **379** (2007) 755–772, [astro-ph/0611671].

[66] A. Bottino, F. Donato, N. Fornengo, and S. Scopel, *Do current WIMP direct measurements constrain light relic neutralinos?*, *Phys. Rev.* **D72** (2005) 083521, [hep-ph/0508270].

[67] A. Bottino, F. Donato, N. Fornengo, and S. Scopel, *Zooming in on light relic neutralinos by direct detection and measurements of galactic antimatter*, *Phys. Rev.* **D77** (2008) 015002, [arXiv:0710.0553].

[68] A. M. Green, *Extracting information about WIMP properties from direct detection experiments: astrophysical uncertainties*, arXiv:1004.2383.

[69] **XENON10** Collaboration, J. Angle *et al.*, *Constraints on inelastic dark matter from XENON10*, *Phys. Rev.* **D80** (2009) 115005, [arXiv:0910.3698].

[70] A. Manzur *et al.*, *Scintillation efficiency and ionization yield of liquid xenon for mono-energetic nuclear recoils down to 4 keV*, *Phys. Rev.* **C81** (2010) 025808, [arXiv:0909.1063].

[71] S. Kraml and D. T. Nhung, *Three-body decays of sleptons in models with non-universal Higgs masses*, *JHEP* **02** (2008) 061, [arXiv:0712.1986].

[72] G. Jungman, M. Kamionkowski, and K. Griest, *Supersymmetric dark matter*, *Phys. Rept.* **267** (1996) 195–373, [hep-ph/9506380].

[73] A. Gould, *WIMP Distribution in and Evaporation from the Sun*, *Astrophys. J.* **321** (1987) 560.

[74] K. Griest and D. Seckel, *Cosmic Asymmetry, Neutrinos and the Sun*, *Nucl. Phys.* **B283** (1987) 681.

[75] M. Cirelli *et al.*, *Spectra of neutrinos from dark matter annihilations*, *Nucl. Phys.* **B727** (2005) 99–138, [hep-ph/0506298].

[76] A. E. Erkoca, M. H. Reno, and I. Sarcevic, *Muon Fluxes From Dark Matter Annihilation*, *Phys. Rev.* **D80** (2009) 043514, [arXiv:0906.4364].

[77] G. Belanger, F. Boudjema, A. Pukhov, and A. Semenov. in preparation.

[78] V. Niro, A. Bottino, N. Fornengo, and S. Scopel, *Investigating light neutralinos at neutrino telescopes*, *Phys. Rev.* **D80** (2009) 095019, [arXiv:0909.2348].

[79] A. A. Abdo *et al.*, *Observations of Milky Way Dwarf Spheroidal galaxies with the Fermi-LAT detector and constraints on Dark Matter models*, *Astrophys. J.* **712** (2010) 147–158, [arXiv:1001.4531].

[80] J. F. Navarro, C. S. Frenk, and S. D. M. White, *The Structure of Cold Dark Matter Halos*, *Astrophys. J.* **462** (1996) 563–575, [astro-ph/9508025].

[81] **PAMELA** Collaboration, O. Adriani *et al.*, *PAMELA results on the cosmic-ray antiproton flux from 60 MeV to 180 GeV in kinetic energy*, arXiv:1007.0821.

[82] F. Donato *et al.*, *Antiprotons from spallation of cosmic rays on interstellar matter*, *Astrophys. J.* **563** (2001) 172–184, [astro-ph/0103150].

[83] D. Maurin, F. Donato, R. Taillet, and P. Salati, *Cosmic Rays below Z=30 in a diffusion model: new constraints on propagation parameters*, *Astrophys. J.* **555** (2001) 585–596, [astro-ph/0101231].

[84] F. Donato, N. Fornengo, D. Maurin, and P. Salati, *Antiprotons in cosmic rays from neutralino annihilation*, *Phys. Rev.* **D69** (2004) 063501, [astro-ph/0306207].

[85] **PAMELA** Collaboration, O. Adriani *et al.*, *An anomalous positron abundance in cosmic rays with energies 1.5-100 GeV*, *Nature* **458** (2009) 607–609, [arXiv:0810.4995].

[86] T. Delahaye *et al.*, *Galactic secondary positron flux at the Earth*, *Astron. Astrophys.* **501** (2009) 821–833, [arXiv:0809.5268].

[87] A. de Roeck, "Higgs physics at the LHC and ILC." Plenary talk at 13th International Conference on Supersymmetry and Unification of Fundamental Interactions (SUSY 2005), IPPP Durham, 18–23 July 2005.

[88] M. Drees, R. Godbole, and P. Roy, *Theory and phenomenology of sparticles: An account of four-dimensional N=1 supersymmetry in high energy physics*, . Hackensack, USA: World Scientific (2004) 555 p.

[89] H. Baer and X. Tata, *Weak scale supersymmetry: From superfields to scattering events*, . Cambridge, UK: Univ. Pr. (2006) 537 p.

[90] **ECFA/DESY LC Physics Working Group** Collaboration, J. A. Aguilar-Saavedra *et al.*, *TESLA Technical Design Report Part III: Physics at an e+e- Linear Collider*, hep-ph/0106315.

[91] H. Baer and A. Belyaev, *Associated neutralino neutralino photon production at NLC*, hep-ph/0111017.

[92] A. Birkedal, K. Matchev, and M. Perelstein, *Dark matter at colliders: A model-independent approach*, *Phys. Rev.* **D70** (2004) 077701, [hep-ph/0403004].

[93] C. Bartels and J. List, *WIMP Searches at the ILC using a model-independent Approach*, arXiv:0901.4890.

[94] K. Murase, T. Tanabe, T. Suehara, S. Yamashita, and S. Komamiya, *Using Single Photons for WIMP Searches at the ILC*, arXiv:1006.3551.

[95] G. Polesello and D. R. Tovey, *Supersymmetric particle mass measurement with the boost-corrected contransverse mass*, *JHEP* **03** (2010) 030, [arXiv:0910.0174].

[96] P. Z. Skands *et al.*, *SUSY Les Houches Accord: Interfacing SUSY Spectrum Calculators, Decay Packages, and Event Generators*, *JHEP* **07** (2004) 036, [hep-ph/0311123].